European Journal of Medicinal Chemistry 251 (2023) 115245

Contents lists available at ScienceDirect

European Journal of Medicinal Chemistry

journal homepage: www.elsevier.com/locate/ejmech

Research paper

C-glycosides analogues of the okadaic acid central fragment exert neuroprotection via restoration of PP2A-phosphatase activity: A rational design of potential drugs for Alzheimer's disease targeting tauopathies

Raquel L. Arribas [a,b], Lucía Viejo [a,c], Isaac Bravo [c,d], Minerva Martínez [a], Eva Ramos [e], Alejandro Romero [e], Eva M. García-Frutos [d,f], Veerle Janssens [g,h], Carmen Montiel [a], Cristóbal de los Ríos [a,b,c,*]

[a] Instituto-Fundación Teófilo Hernando, Universidad Autónoma de Madrid, 28029, Madrid, Spain
[b] Departamento de Ciencias Básicas de la Salud, Universidad Rey Juan Carlos, 28922, Alcorcón, Spain
[c] Instituto de Investigación Sanitaria, Hospital Universitario de la Princesa, C/ Diego de León, 62, 28006, Madrid, Spain
[d] Instituto de Ciencia de Materiales de Madrid, Consejo Superior de Investigaciones Científicas, 28049, Madrid, Spain
[e] Departamento de Farmacología y Toxicología, Facultad de Veterinaria, Universidad Complutense, 28040, Madrid, Spain
[f] Universidad de Alcalá, Departamento de Química Orgánica y Química Inorgánica, Ctra. Madrid-Barcelona Km.33,600, 28871, Alcalá de Henares, Madrid, Spain
[g] Department of Cellular & Molecular Medicine, Laboratory of Protein Phosphorylation and Proteomics, KU Leuven, B-3000, Leuven, Belgium
[h] LBI (KU Leuven Brain Institute), B-3000, Leuven, Belgium

ARTICLE INFO

Keywords:
Alzheimer's disease
Neuroprotection
Okadaic acid
Protein phosphatase 2A (PP2A)
PP2A-activating drug (PAD)
Tauopathies

ABSTRACT

Protein phosphatase 2A (PP2A) is an important Ser/Thr phosphatase that participates in the regulation of multiple cellular processes. This implies that any deficient activity of PP2A is the responsible of severe pathologies. For instance, one of the main histopathological features of Alzheimer's disease is neurofibrillary tangles, which are mainly comprised by hyperphosphorylated forms of tau protein. This altered rate of tau phosphorylation has been correlated with PP2A depression AD patients. With the goal of preventing PP2A inactivation in neurodegeneration scenarios, we have aimed to design, synthesize and evaluate new ligands of PP2A capable of preventing its inhibition. To achieve this goal, the new PP2A ligands present structural similarities with the central fragment C19–C27 of the well-established PP2A inhibitor okadaic acid (OA). Indeed, this central moiety of OA does not exert inhibitory actions. Hence, these compounds lack PP2A-inhibiting structural motifs but, in contrast, compete with PP2A inhibitors, thus recovering phosphatase activity. Proving this hypothesis, most compounds showed a good neuroprotective profile in neurodegeneration models related to PP2A impairment, highlighting derivative **10**, named ITH12711, as the most promising one. This compound (1) restored *in vitro* and cellular PP2A catalytic activity, measured on a phospho-peptide substrate and by western-blot analyses, (2) proved good brain penetration measured by PAMPA, and (3) prevented LPS-induced memory impairment of mice in the object recognition test. Thus, the promising outcomes of the compound **10** validate our rational approach to design new PP2A-activating drugs based on OA central fragment.

1. Introduction

Phosphoprotein phosphatase 2A (PP2A) is a key family of cellular enzymes catalyzing the hydrolysis of phosphate esters at phospho-Ser and phospho-Thr residues. It is implicated in the fine regulation of the phosphorylation/dephosphorylation balance of a myriad of cellular proteins (its substrates) [1], underscoring its essential role in a plethora of physiological processes of eukaryotes [2], including cell cycle control [3], cell proliferation and death [4,5], metabolism [6] and cytoskeleton dynamics [7]. Structurally, PP2A enzymes are heterotrimeric complexes formed by a dimeric core composed of a scaffolding subunit (PP2A-A), a catalytic subunit (PP2A-C), and a variable regulatory subunit (PP2A-B), the latter being responsible for the substrate specificity and organ localization [8,9]. Indeed, there are nearly 100 heterotrimeric holoenzymes, as result of the combination of different isoforms expressed for each subunit [8,9]. PP2A activity is further regulated by post-translational mechanisms, including reversible PP2A-C

* Corresponding author. Departamento de Ciencias Básicas de la Salud, Universidad Rey Juan Carlos, 28922, Alcorcón, Spain.
E-mail addresses: cristobal.delosrios@inv.uam.es, cristobal.delosrios@urjc.es (C. de los Ríos).

https://doi.org/10.1016/j.ejmech.2023.115245
Received 31 October 2022; Received in revised form 24 January 2023; Accepted 28 February 2023
Available online 4 March 2023

Abbreviations

AD	Alzheimer's disease
Aβ	Amyloid β
APP	Aβ precursor protein
BBB	blood-brain barrier
C	caffeine
CNS	central nerve system
FBS	fetal bovine serum
GFP	green fluorescent protein
LPS	lipopolysaccharide
Mem	memantine
NFT	neurofibrillary tangles
NMDAr	*N*-methyl-D-aspartate-sensitive glutamate receptors
OA	okadaic acid
PAD	PP2A-activating drug
PAMPA	parallel artificial membrane permeation assays
PME-1	protein phosphatase methyl esterase 1
*p*NPP	para-nitrophenol phosphate
PP2A	protein phosphatase 2A
ppm	parts per million
PPP	phosphoprotein phosphatases
R/O	rotenone plus oligomycin A
SAR	structure-activity relationships
SMAP	small molecule activator of PP2A
T	testosterone

carboxymethylation [10,11], and PP2A-C or B subunit phosphorylation [9,12]. In addition, several endogenous polypeptides inhibit PP2A by direct interaction [13]. Amongst these, $I2^{PP2A}$/SET [14] and CIP2A [15] stand out, because their hyperactivity, cell translocation or aberrant overexpression appear pathogenic, causing several types of cancer or various neurodegenerative diseases [15,16].

Gathering all this knowledge, the early simplified view considering protein phosphatases such as PP2A, as promiscuous and unspecific enzymes without pharmacological interest, is fully overcome [17]. Nowadays, PP2A and other protein phosphatases are taken as very promising therapeutic targets for many human diseases [18]. In particular, PP2A has received vast attention in the latest years because of two main reasons. Firstly, by its widely recognized role as tumor suppressor [8,19,20] and its decreased activity in many cancer types, including lung [21], colorectal [22], breast [23], hepatic cancers [24], and leukemias [25,26]. Secondly, by its key role in the dephosphorylation of the microtubule-stabilizing tau protein [27,28], thereby preventing tauopathies such as Alzheimer's disease (AD). One of the morphological hallmarks of AD is the presence of the so-called neurofibrillary tangles (NFT), aberrant aggregates formed by hyperphosphorylated tau protein [29]. The tauopathy-modulating behavior of PP2A does not only involve its ability to directly dephosphorylate tau [28], but also dephosphorylates several tau kinases, such as GSK-3β, ERK1/2 and JNK, regulating their action [30,31]. Furthermore, PP2A dephosphorylates amyloid β (Aβ) precursor protein (APP) at Thr668 [32], thus hindering the APP proteolytic processing and Aβ synthesis [33]. Finally, PP2A dephosphorylates several kinases controlling inflammatory or stress signaling pathways to dissipate inflammation [34,35] and promote the viability of neuroprotective M2 microglia [36], or p47phox, whose dephosphorylation inactivates the whole NADPH oxidase complex to reduce oxidative stress [37]. Another stress kinase is MAP3K dual leucine zipper (DLK), overexpressed in AD brains [38], which is inhibited by PP2A in neurons [39]. Corroborating its relevance in protection against neurodegeneration, PP2A appears depressed, inhibited or inactivated in AD patients' brains [40] and inhibition of its function in animal models results in neurodegenerative phenotypes [40]. For all of these reasons, pharmacological activation or re-activation of PP2A has become a valuable strategy for drug development in AD [41].

In the last decade, various approaches have been undertaken to reach these goals [17]. The majority of examples have been addressed to indirectly (re)activate PP2A, by inhibiting its cellular inhibitors,

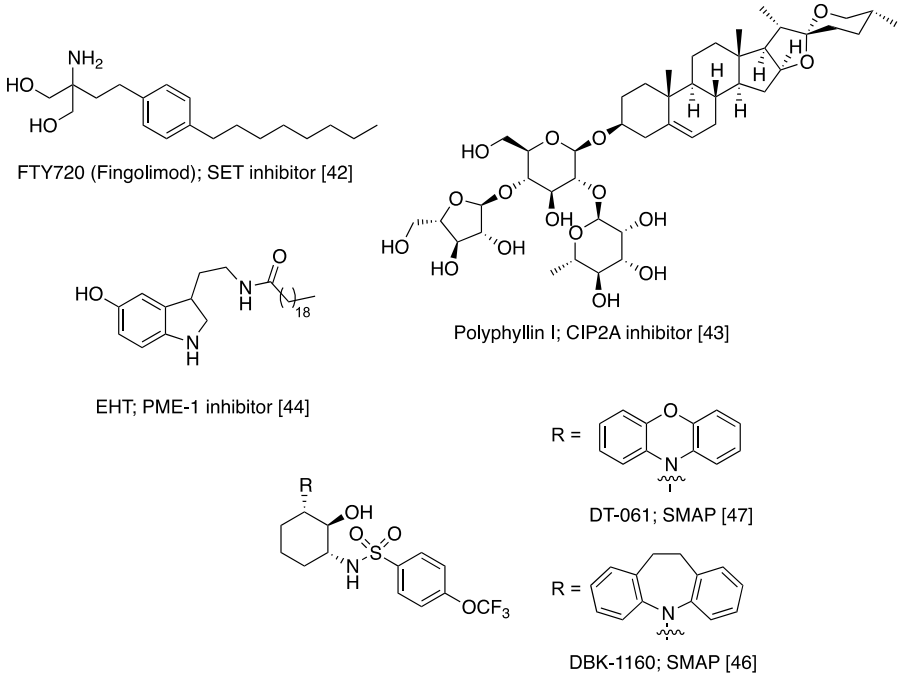

Fig. 1. Selected recent PP2A-activating drugs studied for neurodegenerative diseases. (1.5 COLUMN FITTING FIGURE).

including I2/SET [42], CIP2A [43] and PME-1 [44] (Fig. 1). More recent contributions have focused on directly potentiating PP2A activity [45], highlighting phenothiazine derivatives and tricyclic sulfonamides, discovered from chemical library screenings [46], as small molecule activators of PP2A (SMAPs) [47] (Fig. 1). In addition, complex natural products have also been suggested to activate PP2A, such as polyphyllin I [43] (Fig. 1), cornel iridoid glycosides [48], Gingko Biloba extract [49] or pseudoginsenoside-F11 [50]. Overall, the direct PP2A-activating drug (PAD) that has reached the highest level of clinical trial up to date has been sodium selenate, known as VEL-015 [51].

For more than a decade, our research group has been interested in developing new direct PADs through rational drug design-based methodologies, backed up by computational docking [52]. Like that, we reported a 1,8-naphthyridine derivative (Fig. 2) [53] and a family of 3-aminomethylindoles [54] and azaindoles [55], showing both PP2A recovery capabilities and interesting neuroprotective profiles in several *in vitro* and *in vivo* models of AD. To obtain more potent and selective PADs, we recently focused on the chemical structure of okadaic acid (OA), the best-known PP2A selective inhibitor [56] (Fig. 2).

This toxin has been the object of deep structure-activity relationship (SAR) studies [57], showing that the central cyclic fragment (C19–C27) and the one at the spiroketal edge (C30–C38) (Fig. 2) do not participate in the inhibitory effect of OA, as they interact with amino acids far from the PP2A-C catalytic triad. Instead, they increase the affinity of OA for the PP2A-C subunit [58,59]. Hence, we hypothesized that small molecules mimicking these two cyclic fragments might still bind, but no longer inhibit PP2A-C. In addition, this particular interaction might also prevent PP2A inhibitors, either endogenous ones or toxins, could get close to PP2A; or that toxin- or cellular inhibitor-inhibited PP2A enzymatic activity could be restored. This hypothesis was recently underscored by the chemotherapeutic potential of a *C*-glycoside small analogue to OA C19–C27 fragment, named ITH12680 (**1**) (Fig. 2), which resensitized non-small cells lung cancer cells to cisplatin treatment in a model of chemoresistance, via a mechanism that restored PP2A activity [60]. In the current study, we report improved *C*-glycoside analogues of the OA C19–C27 fragment, and their neuroprotective potential in neurodegeneration models related to pathologic tau hyperphosphorylation.

2. Results and discussion

2.1. Chemistry

The design of *C*-glycosides with potential PAD ability was based on the OA central fragment C19–C27, maintaining the absolute configuration of analogous stereocenters (Fig. 2). In some examples, we pursued increasing structural rigidity by tightening the exocyclic oxygen atoms through cyclic acetals. The drugability of designed compounds was maintained according to physicochemical properties related to Lipinski's rule of five (Table S1, supplementary material). To furnish the desired entities, we have taken advantage of the Organic Chemistry literature centered on pursuing the total synthesis of OA [61–63] and other dinophysistoxins [64], where the contributions of Forsyth's group have been crucial.

Compound **1**, prepared following the Hosomi-Sakurai reaction [60], was subjected to basic hydrolysis with sodium methoxide to afford diol **2** in quantitative yield (Scheme 1). Classical methods recruiting milder hydrolyses such as the use of TEA [61] were less efficient. As discussed above, rigidity was achieved by the generation of cyclic acetals, which also dissipated the high hydrophilicity of **2** (clog P = 0.3). First, the reaction of **2** with benzaldehyde dimethylacetal according to Isobe's conditions yielded compound **3** in medium yields (Scheme 1). Despite the fact that acetal **3** showed sensibility to aqueous acid media, the use of neutralized solvents sorted out its potential instability. The acetal **4**, which presents an acetonide structure, was obtained from reaction of **2** with 2-methoxypropene under mild acid catalysis in quantitative yield (Scheme 1), which exhibited increased stability.

Then, with the purpose of resembling the oxygen at C19 of OA (Fig. 2), compounds **3** and **4** were hydroxylated under hydroboration/oxidation conditions. Unlike what was reported in the literature, treatment with diborane was unsuccessful in any of the experimental conditions tested. Better outcomes were achieved with 9-BBN, as its reaction with the benzylidene derivative **3** provided alcohol **5** (Scheme 2), although chromatographic purification was rather complicated. Only the use of a preparative TLC allowed to isolate alcohol **5** in low yields. The more stable acetonide **4** yielded alcohol **6** in good yields (82%, Scheme 2) after regular automatized chromatography. Noteworthy, beyond the left side of the OA C19–C27 fragment, the own C19 shows a diol substructure. Hence, we wondered whether a non-classical isosteres

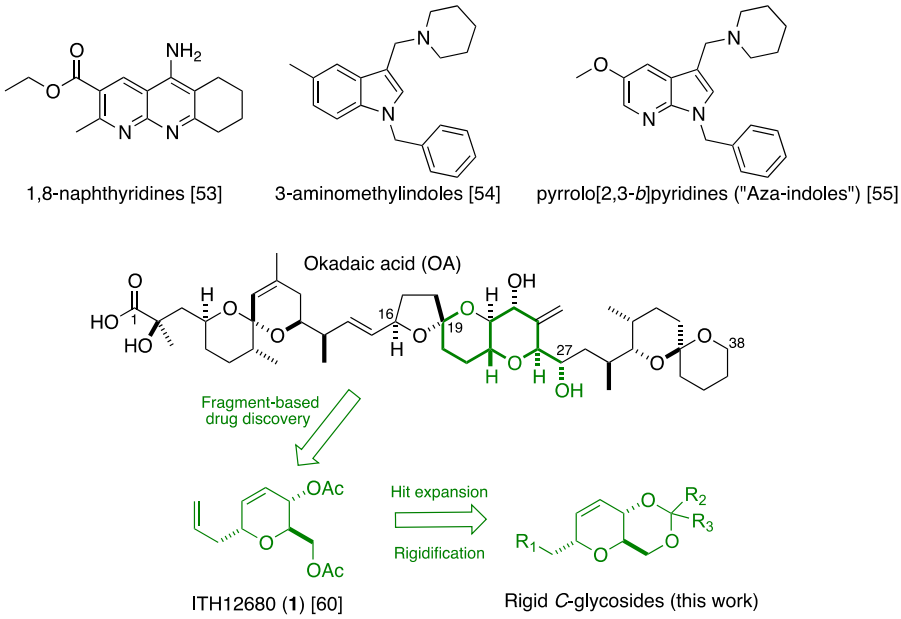

Fig. 2. PADs described by our research group and design of the new family based on the OA central fragment. (FIGURE IN COLOR, 1.5 COLUMN FITTING FIGURE).

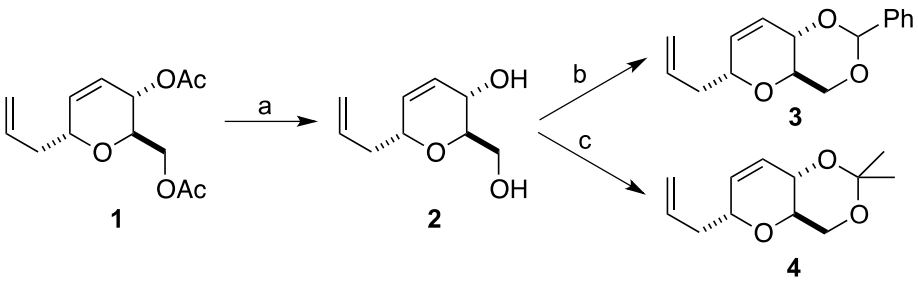

Scheme 1. Strategies of annulation of the alcoholic groups at *C*-glycosides analogues to OA C19–C27 fragment. Reagents and conditions: (a) MeONa/MeOH, rt, 16 h; (b) benzaldehyde dimethyl acetal, CSA, 1,2-DCE, rt, 16 h; (c) 2-methoxypropene, PPTS, DCM, 0 °C to rt, 5 h (1.5 COLUMN FITTING SCHEME).

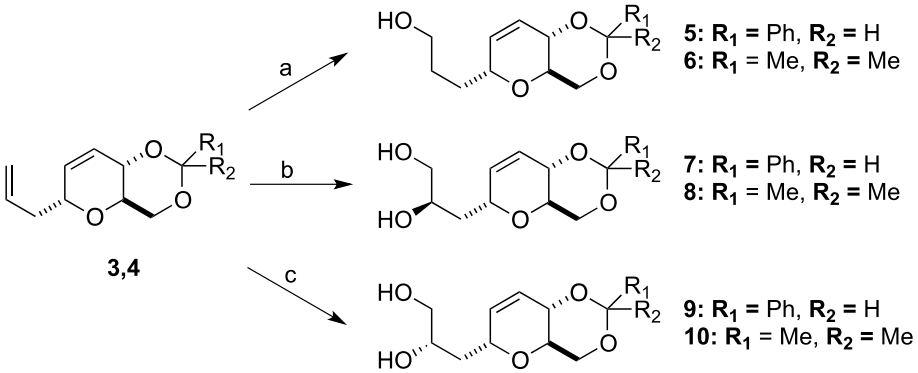

Scheme 2. Strategies of hydroxylation of the rigid *C*-glycosides analogues to OA C19–C27 fragment. Reagents and conditions: (a) i. 9-BBN, THF, rt, 1 h. ii. H_2O_2/$NaOH_{aq}$, rt, 0.5 h; (b) AD-mix-β, $^tBuOH/H_2O$, 0 °C, 6 h; (c) AD-mix-α, $^tBuOH/H_2O$, 0 °C, 6 h (SINGLE COLUMN FITTING SCHEME).

strategy to build a 1,2-diol moiety could furnish bioactive compounds. For that purpose, Sharpless asymmetric dihydroxylation [65] allowed us to obtain derivatives possessing vicinal diols with high stereoselectivity from alkenes **3** and **4**.

The reaction of alkenes **3** (R_1 = Ph, R_2 = H) and **4** (R_1, R_2 = Me) with AD-mix-β resulted in the formation of 1,2-diols **7** and **8**, respectively, possessing *R* configuration at C2 with high stereoselectivity and very good yields. Under similar experimental conditions, the commercial reagent AD-mix-α afforded the (*2S*)-alkenes **9** and **10** with good yields and very good stereoselectivity. AD-mix reagents α and β oppositely exert syn-dihydroxylations asymmetrically ruled by the *cis*-trans isomerism of the olefinic substrate. However, the stereoselective discrimination between both pro-chiral faces is not so obvious in monosubstituted alkenes such as **3** and **4**. For this reason, we have confirmed the stereoselectivity of AD-mix reagents by X-Ray diffraction (Fig. S1, supplementary material) using compound **10** as a model.

During the pharmacological evaluation of target compounds and subsequent computational docking studies, we considered of interest the benzoylation of mono-alcohols **5** and **6**. Treatment with BzCl in pyridine generated benzoates **11** and **12** with very low yields (Scheme 3). Trends with stronger bases were unsuccessful. For instance, the use of K_2CO_3 as a base led to the diacetal **6** deprotection along benzoylation, yielding compound **13** (Table 1).

2.2. Analogues to OA central fragment 1–13 mitigated OA and cytostatin-induced protein phosphatases inhibition in SH-SY5Y cells

The SH-SY5Y neuroblastoma cell line is a well-described model to estimate the effect of potential PADs, as it draws a readable phosphatase activity that is sensitive to the presence of PP2A selective inhibitors: exposure of SH-SY5Y cells to the selective inhibitor OA at 15 nM for 18 h indeed diminished the *para*-nitrophenyl phosphate (*p*NPP)-measured phosphatase activity by 29% (Fig. 3).

As shown in Fig. 3, most of the *C*-glycosides tested, administered at a concentration of 1 μM to SH-SY5Y cells, counteracted the OA-induced drop of phosphatase activity by 50% or more (Fig. 3 and Table S1, supplementary material). In general, rigidified compounds with benzylidene moiety outperformed their acetonide analogues, except for compound **10**, which was the best PAD, together with benzylidene derivative **7**. Only diol **13**, which bears a long benzoyl group, was unable to antagonize OA inhibitory actions. Similarly, the incorporation of a benzoyl in **11** and **12** was unfruitful for PP2A recovery activity, compared with the corresponding free alcohol analogues **5** and **6**. The AD drug memantine was used as standard in these experiments, considering its pro-activating profile of PP2A [66] independent of the blockade of *N*-methyl-D-aspartate-sensitive glutamate receptors (NMDAr).

Although the cellular manifestations caused by nanomolar concentrations of OA are generally ascribed to its inhibitory effect on PP2A [67], a possibility exists that it could affect other PPP with a less

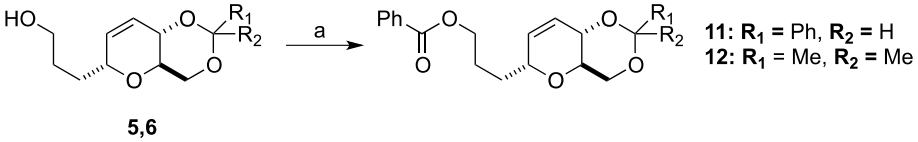

Scheme 3. Benzoylation of alcohols **5** and **6**. Reagents and conditions: (a) BzCl, Py, rt, 18 h (SINGLE COLUMN FITTING SCHEME).

Table 1
Percentage of neuroprotection offered by *C*-glycosides **1**–**13** administered to cell cultures at the concentration of 1 μM on cell viability measured by the MTT assay in various *in vitro* models of neurodegeneration.

	Okadaic acid[a]	*Cytostatin*[b]	*R/O*[c]	*Glutamate*[d]
Memantine	60 ± 2***	57 ± 5**	–	22 ± 2**
Melatonin	–	–	28 ± 2***	–
1	84 ± 2***	47 ± 4**	23 ± 4*	19 ± 2**
2	72 ± 6*	45 ± 5*	30 ± 5*	15 ± 2*
3	80 ± 4***	49 ± 5*	26 ± 1**	15 ± 2*
4	50 ± 1***	50 ± 5*	63 ± 3***	8 ± 6
5	82 ± 3***	52 ± 7*	29 ± 4*	12 ± 3
6	81 ± 6**	45 ± 5*	5 ± 3	6 ± 2
7	40 ± 8	21 ± 7	10 ± 3	29 ± 6*
8	45 ± 8	56 ± 6*	24 ± 2**	15 ± 1*
9	73 ± 2***	54 ± 5**	27 ± 2**	13 ± 1*
10	72 ± 5**	64 ± 5**	16 ± 2*	20 ± 4*
11	72 ± 5**	47 ± 5*	7 ± 1	8 ± 2
12	69 ± 5**	37 ± 3*	15 ± 5	17 ± 3*
13	20 ± 8	1 ± 6	3 ± 4	17 ± 3*

***$P < 0.001$, **$p < 0.01$, *$p < 0.05$, compared with percentage of viability of the corresponding toxic stimulus in absence of compounds. Data are expressed as mean of %protection ± SEM of at least 4 independent experiments.

[a] SH-SY5Y neuroblastoma cells stimulated with okadaic acid 20 nM.

[b] SH-SY5Y neuroblastoma cells stimulated with cytostatin 2.5 μM.

[c] SH-SY5Y neuroblastoma cells stimulated with rotenone 30 μM plus oligomycin 10 μM (R/O).

[d] Embryonic rat cortical neurons subjected to glutamate 50 μM. (SINGLE COLUMN FITTING TABLE).

physiological role in the central nervous system, such as PP1, PP4 or PP5 [56,68]. To corroborate that activity of compounds **1**–**13** was directly related to a PP2A restoring profile, we repeated *p*NPP-based experiments using the toxin cytostatin, which is a less potent but much more selective PP2A inhibitor [68]. SH-SY5Y cells treated with cytostatin at 2 μM diminished their *p*-NPP-probed phosphatase activity by 28% (Fig. 4). In a quite similar fashion to that observed in the previous experiment with OA, most of the assayed *C*-glycosides dissipated the inhibitory effects of cytostatin on SH-SY5Y cells by around 50%. The best antagonist compound against cytostatin was diol **2**. Again, the incorporation of benzoyl was detrimental for PAD activity. In some cases, acetonides worsened recovery of phosphatase activity compared with benzylidene analogues, but this was not so obvious in diols **7**–**10**. Indeed, these *C*-glycosides presenting a 1,2-diol group from Sharpless' dihydroxylation presented a very robust PAD capacity (Figs. 3 and 4).

2.3. Analogues to OA central fragment *1*–*13* protected in vitro neuronal models against several toxic stimuli related to neurodegeneration

Prior to assessing the neuroprotective effects of the compounds **1**–**13** at *in vitro* models of neurodegeneration, we confirmed that *C*-glycosides *per se* lacked toxicity in a wide range of concentrations, measured with the method of MTT reduction (Fig. S2, supplementary material). A tiny reduction of cell viability is only observed upon the use of compound **2** at a concentration of 30 μM (Fig. S2, supplementary material). Next, we evaluated whether the PAD activity of compounds **1**–**13** exerted neuroprotection in neuronal *in vitro* models damaged with several toxic stimuli related to neurodegeneration. Because of its high inhibitory capacity of PPP, mainly of PP2A, OA has been widely used to resemble AD manifestations in particular, but tauopathies in general, in both *in vitro* and *in vivo* models [54–56,67]. For instance, it has been described that SH-SY5Y neuroblastoma cultures show a loss of cell viability when challenged with OA at nanomolar concentrations during several hours of incubation [69]. A 20 h-exposition of SH-SY5Y cells to OA 20 nM indeed provoked a loss of about 30% in cell viability, measured by the MTT colorimetric dye, of about 30%. In this situation, compounds **1**–**13**, pre-incubated (24 h) and co-incubated at 1 μM with OA 20 nM, protected SH-SY5Y cells from OA-induced cell death in a statistically significant fashion, except **7, 8** and **13** (Table 1). Stereochemistry at C2 dramatically influenced neuroprotection *vs* OA. The reference drug memantine was used as standard in the PP2A inhibition-derived neuroprotection experiments [66].

On the other hand, cytostatin has not been object of extensive research as an inducer model of neuronal death. Nevertheless, we found that it was a very reliable and straightforward tool to support and reinforce that the neuroprotective properties of the target compounds **1**–**13** are directly related to PP2A restoring activity. Thus, cytostatin, added to SH-SY5Y cells at 2.5 μM for 20 h, provoked a 35% drop of cell viability, monitored by the MTT assay. Again, most *C*-glycosides tested mitigated the neuronal damage induced by cytostatin (Table 1), as only compounds **7** and **13** failed, while the 1,2-diol acetonide derivative **10** provided the best neuroprotection.

One of the most relevant features of PP2A is the control of neuroinflammation and oxidative stress, as it down-regulates several neurodegeneration-leading inflammatory mediators, by dephosphorylation [34,37]. For this reason, we found of interest to test the neuroprotective profile of compounds **1**–**13** in an *in vitro* model of oxidative stress, induced by 30 μM rotenone/10 μM oligomycin A (R/O). Rotenone and oligomycin A inhibit complexes I and V of the mitochondrial

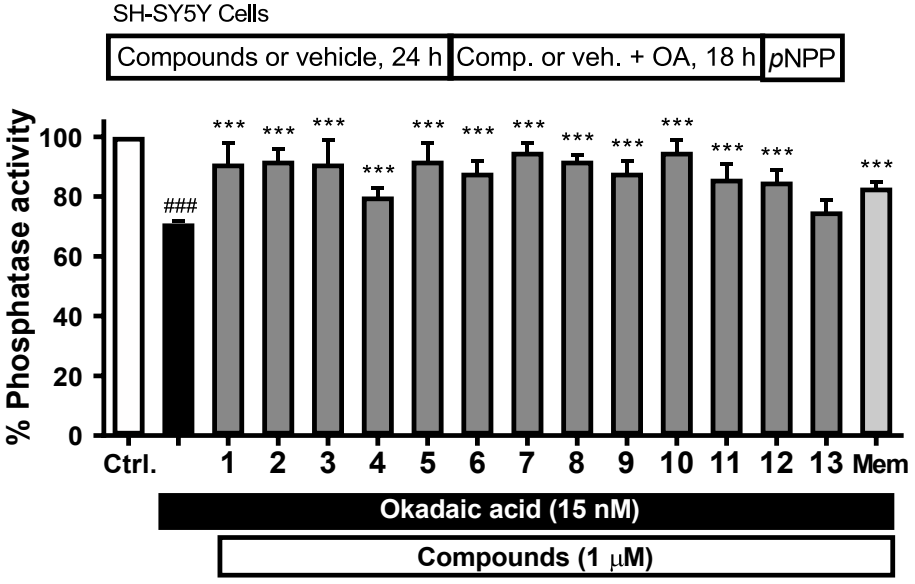

Fig. 3. Percentage of phosphatase activity, measured by the *p*NPP method, in SH-SY5Y cells. After 24 h of incubation with the compounds, SH-SY5Y cells were exposed to OA 15 nM and 1 μM of compounds for 18 h. Memantine (Mem), used as standard, was administered at 10 nM. Data are expressed as mean ± SEM of at least 4 independent experiments, normalized versus phosphatase activity of control (Ctrl, white bar*), i.e.* SH-SY5Y cells non-treated with OA in absence of compounds (Ctrl). ###$P < 0.001$, relative to Ctrl; ***$p < 0.001$, relative to SH-SY5Y cells exposed to OA in absence of compounds (black bar). (1.5 COLUMN FITTING FIGURE).

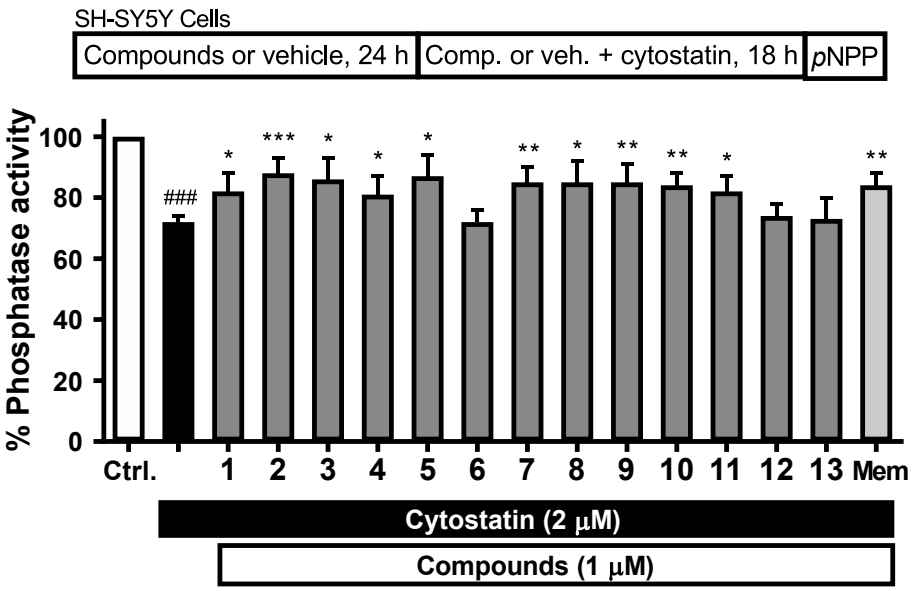

Fig. 4. Percentage of phosphatase activity, measured by *p*NPP method, in SH-SY5Y cells. Effect of derivatives **1**–**13** on PP2A phosphatase activity. After 24 h of incubation with compounds, the SH-SY5Y cells were exposed to 2 μM cytostatin and 1 μM of compounds for 18 h. Memantine (Mem), used as a standard, was administered at 10 nM. Data are expressed as mean ± SEM of at least 3 independent experiments, normalized versus phosphatase activity of control (Ctrl, white bar*), i.e.* SH-SY5Y cells non-treated with OA in absence of compounds (Ctrl). $^{###}P < 0.001$, relative to Ctrl; $^{***}p < 0.001$, relative to SH-SY5Y cells exposed to OA in absence of compounds (black bar). (1.5 COLUMN FITTING FIGURE).

electron transport chain, respectively, triggering reactive oxygen species generation, mitochondrial dysfunction, and ATP synthesis lockout [70]. Application of the R/O cocktail to SH-SY5Y cells for 24 h resulted in a cell viability decay of 40%. The pre- and co-incubation with the *C*-glycosides at 1 μM protected the neuroblastoma cultures against cell damage by R/O in 8 out of the 13 compounds probed, with the largest effect seen for alkene **4** (Table 1). Although they have not been designed as antioxidants, the fact that this family of PADs exhibited a neuroprotective profile against oxidative stress underlines the important role of PP2A in the regulation of the cellular redox state. In this respect, the incorporation of a benzoyl moiety in compounds **11**–**13** impaired the antioxidant properties of this series, while the presence of a pending vinyl group promoted this, presumably because of the scavenging character of accessible double bonds.

The last cell model we used to test our compounds was based on the excitotoxicity suffered by neuronal cultures exposed to high and sustained concentrations of glutamate, *i.e.* 50 μM, which can be found in the cerebrospinal fluid of patients with neurodegenerative disorders [66], leading to overstimulation of NMDAr and neuronal cell death [71]. The value of this experimental model lies in the fact that PP2A regulates NMDAr signaling [72], for instance, by dephosphorylation of its NR1 subunit, thereby desensitizing it. So, a potential PP2A activator should hinder the neurotoxic events derived from glutamate exposure. Since SH-SY5Y neuroblastoma cells lack functional NMDAr [73], we used embryonic rat cortical neurons to evaluate potential neuroprotective effects exerted by *C*-glycosides **1**–**13** against glutamate excitotoxicity. First, the compounds were incubated with cortical neurons in the absence of glutamate to monitor any *per se* toxicity in this model (Fig. S3, supplementary material). Only **11** and **8**, with no-significance in this case, slightly diminished neuronal viability at 30 μM. Next, we repeated these experiments in the presence of glutamate. While glutamate decreased cell viability by 48%, two thirds of the compounds protected cortical neurons against this toxic stimulus in a statistically significant fashion (Table 1). Again, the family of 1,2-diols **7**–**10** showed the best protective effect, as they increased glutamate-challenged cortical neuron viability by about 20%, similarly to the NMDAr antagonist memantine.

In conclusion, most of the *C*-glycosides analogues to the OA central fragment studied herein, showed a wide-spectrum neuroprotective profile and a good ability to restore or increase PP2A enzymatic activity. Among all derivatives examined, the *C*-glycosides **1, 3, 9** and **10** outstood, for (1) developing neuroprotection in all the models tested, for (2) preventing the OA or cytostatin-induced PP2A inhibition, and for (3) lacking toxicity *per se* in a wide range of concentrations. Of these four compounds, compound **10** was further selected for additional follow-up studies that aimed to deepen its pharmacological and safety profile and its mechanism of action, since it resulted in the highest restoration of OA-inhibited PP2A activity (Fig. 3), and the best protective effect against cytostatin-induced neurotoxicity (Table 1).

*2.4. Rigid analog to OA central fragment **10** reduced the OA-induced inhibition of PP2A- B55α and PP2A- B56α isolated from transfected HEK-293T cells*

We further confirmed the PP2A-recovering capability of compound **10** by carrying out *in vitro* phosphatase activity measurements on purified PP2A complexes using a canonical phospho-peptide substrate (K-R-*p*T-I-R-R) through the Malachite Green method (Fig. 5). Two different PP2A trimeric complexes were analyzed, one harboring the B55α (or Bα) isoform, which is the chief regulatory enzyme of tau dephosphorylation [74], and one encompassing the B56α (or B'α) subunit, which down-regulates major tau kinases, such as ERK1/2 [75]. Both PP2A trimers were isolated by GFP-trapping from HEK-293T cells transfected with GFP-tagged B-type subunits, as described [60]. Since these trimers manifested a slightly different sensitivity to OA, the transfected cells were subjected to a slightly different concentration of the toxin, which resulted in both cases in a detectable and significant reduction of phosphatase activity. As shown in Fig. 5, PP2A-B55α and PP2A-B56α showed a time-dependent inhibition of about 20–30% when isolated from cells challenged with 15 and 20 nM OA, respectively. Noticeably, the rigid *C*-glycoside **10**, administered at 1 μM, partially recovered OA-inhibited PP2A enzymatic activities (Fig. 5), with a higher efficiency towards PP2A-B55α than over PP2A-B56α.

*2.5. Compound **10** prevented the OA-induced increase of tau and GSK-3β phosphorylation in SH-SY5Y cells*

We next wondered whether the rigid glycoside **10** would also be able to modulate the phosphorylation levels of two phosphoprotein substrates of PP2A in SH-SY5Y cells: tau and GSK-3β. Western-blot experiments corroborated increased tau phosphorylation at amino acids Ser202 and Thr205 upon 20 h of OA treatment (Fig. 6A). Increased phosphorylation at these sites is commonly found in NFT [28]. The presence of the *C*-glycoside **10** prevented OA-induced tau

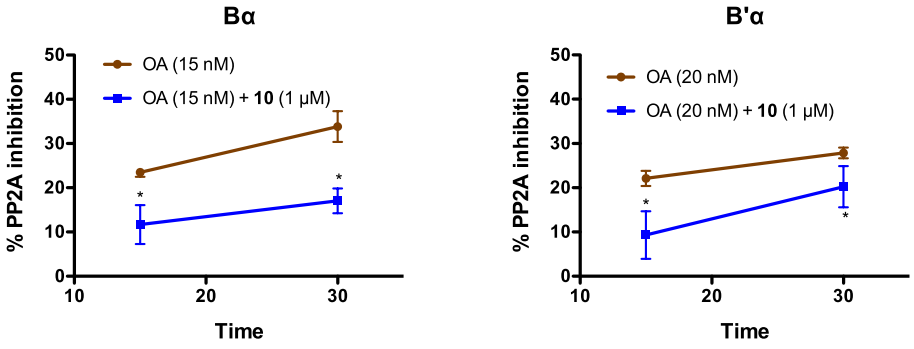

Fig. 5. Percentage of PP2A inhibition measured by the Malachite Green method. PP2A-Bα and PP2A-B'α were purified by pull-down from HEK-293T cells transfected with either GFP-B55α (Bα) or GFP-B56α (B'α), where the GFP was used as a bait and the subunits trapped endogenous PP2A A and C subunits, to assemble into active PP2A trimers. PP2A Bα expressing cells and B'α expressing cells were treated with OA 15 and 20 nM, respectively, and compound **10** at 1 μM. PP2A trimer-induced phosphohydrolysis of the K-R-*p*T-I-R-R phosphopeptide was monitored for 15 and 30 min. Bars show %inhibition ±SEM relative to PP2A activity of trimers isolated from vehicle-treated cells only, and of five independent experiments. $^{*}P < 0.05$. (SINGLE COLUMN FITTING FIGURE, FIGURE IN COLOR).

hyperphosphorylation by half (Fig. 6A). Since it is well-known that PP2A dephosphorylates these pro-aggregating amino acids in tau [76], we might speculate that the administration of PADs like *C*-glycoside **10**, by up-regulating PP2A, might prevent NFT formation, thereby counteracting tauopathy progression. In addition, PP2A regulates the enzymatic activity of several tau kinases. We found that *C*-glycoside **10** may also intervene with this regulation mechanism, since it also inhibited OA-induced GSK-3β hyperphosphorylation at Ser9 (Fig. 6B).

2.6. Computational docking of *10* on PP2A catalytic subunit

Backed by the promising PAD profile of **10**, and with the aim of figuring the structural clues of its interaction to PP2A, we ran docking studies on the catalytic subunit PP2A-C. PP2A crystal structure was obtained from the Protein Data Bank (www.rcsb.org, 2IE4) [57]. Under its lowest energy conformation, compound **10** is posed at a binding pocket formed by amino acids Gln122, Ile123, Val 189, Pro190 and His191 (Fig. 7A). The OA fragments C19–C27 and C30–C38 also present high affinity for these amino acids [57]. Electrostatic view (Fig. 7B) shows that alcohols at C1 and C2 of **10** are accommodated at a positive-charged area, whilst methyl groups are projected to a neutral area formed by Ile123, Gln122 and Val126. Fig. 7C illustrates possible interactions of **10** with this binding pocket. Methyl groups face to a neutral area, generating hydrophobic interactions with Ile123 and the hydrocarbon skeleton of Gln122. Several H-bonds (Fig. 7C, dashed green lines) can be detected, where the strongest is that between C1(*S*)–OH as a donor and the carbonyl of Pro190 (1.91 Å). This OH also H-bonds as a donor with the Cys196 sulfur (2.86 Å) and, as an acceptor, with the Trp200 indole NH (2.80 Å). These interactions could explain the good results of the dihydroxylated derivatives **7**–**10**, but also the slightly better behavior of **10** compared with **8**. In addition, the electronically dense glycosidic oxygen H-bonds the positively charged His191 (3.12 Å). A weak but intramolecular (therefore favored) H-bond appears between C1–OH and one of the dioxin oxygen atoms (3.81 Å). This intramolecular interaction could be the driving force for the shape of the hydrocarbon chain of **10**, placed behind the *C*-glycoside cycle, influencing pharmacological properties. To probe this hypothesis, compounds **11**–**13** were synthesized. Since they proved to be the worst PAD of the family, such hypothesis would prevail.

2.7. Compound *10* shows a high probability of CNS penetration

Based on its pharmacological properties, compound **10** seems an appropriate drug for further *in vivo* studies and preclinical assays.

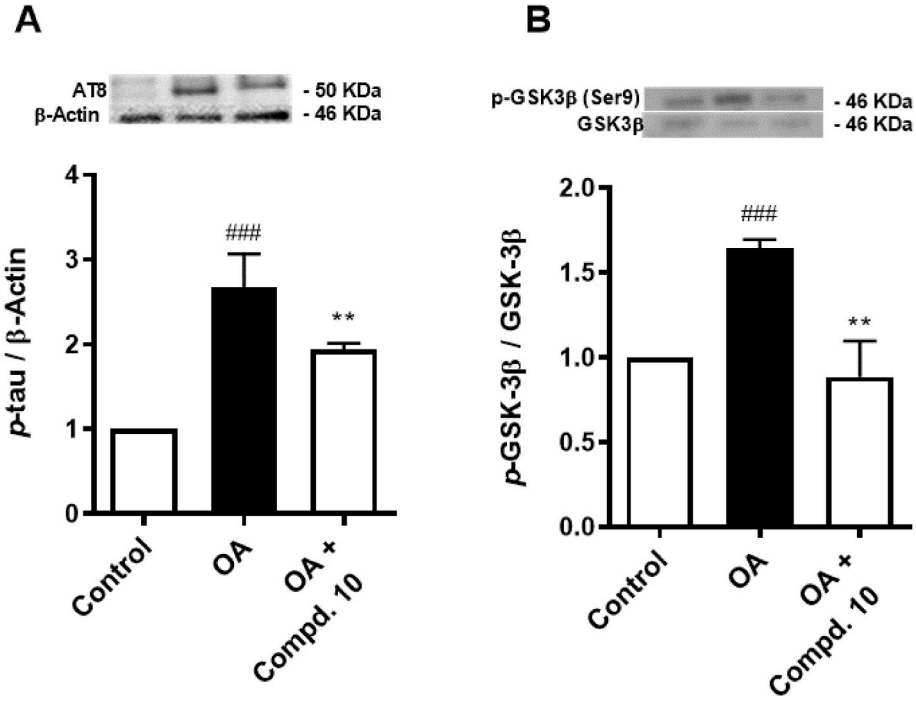

Fig. 6. Protein expression analyses of *p*Tau (Ser202, Thr205) and *p*GSK-3β (Ser9) in SH-SY5Y cells. After 24 h preincubation of compound **10** at 0.1 μM, SH-SY5Y cells were incubated with OA 20 nM or OA 20 nM plus **10** for 20 h more. Top of the graphs, representative immunoblots. Quantitative analysis of the tau phosphorylation (panel **A**) with *anti-p*Tau AT8 that recognizes phosphoepitopes *p*Ser202 and *p*Thr205 of Tau, and of GSK-3β phosphorylation (panel **B**) with phospho-GSK-3β antibody that recognizes the phosphoepitope *p*Ser9 of GSK-3β. Bars represent means ± SEM of at least 3 independent experiments. $^{###}P < 0.001$, $^{##}p < 0.01$ relative to non-treated SH-SY5Y cells (white bars); $^{**}p < 0.01$, $^{*}p < 0.05$, relative to SH-SY5Y exposed only to 20 nM OA alone (black bars). (1.5 COLUMN FITTING FIGURE).

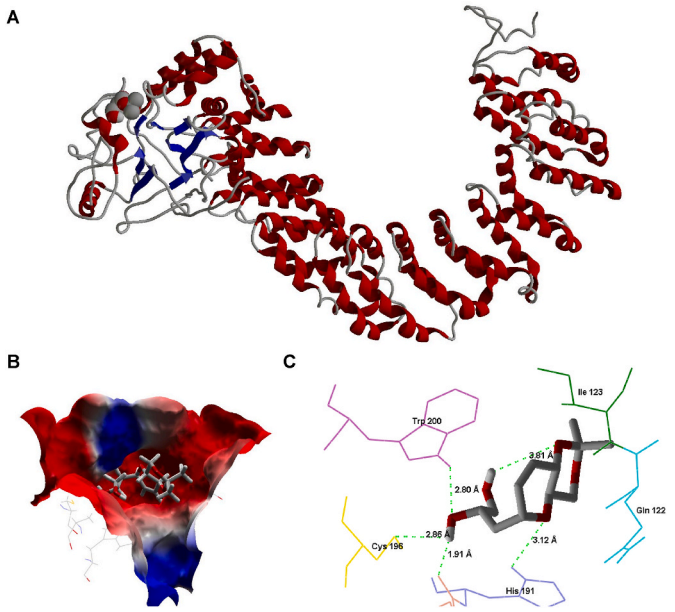

Fig. 7. (**A**) Ribbon-like view of PP2A (PDB: 2IE4) backbone (α-helixes in red and β-sheets in blue); compound **10** represented as CPK-colored space-filled ligand. (**B**) Representation of the electrostatic interactions of compound **10** (CPK-colored sticks) at its binding pocket (red color: negative-charged areas; blue color: positive-charged areas). (**C**) Residues (colored by amino acid type) defining the binding pocket of compound **10**. Hydrogen bonds are shown as dashed green lines along their length. PP2A 3D structure (PDB ID: 2IE4) was obtained from the protein data bank (www.rcsb.org). (DOUBLE COLUMN FITTING FIGURE, FIGURE IN COLOR).

However, even the most suitable pharmacodynamic properties of a drug are worthless unless it can reach its site of action. Since the entire family of designed compounds, including **10**, fulfill the Lipinski's rule of five, we expect them to show an appropriate bioavailability. However, as these compounds need to be able to exert their pharmacological activity within the central nervous system (CNS) and therefore, to cross the highly lipophilic blood-brain barrier (BBB), we carried out parallel artificial membrane permeation assays (PAMPA) [77] in the presence of a lipid extract of porcine brains (Fig. 8). The results show that compound **10** proves a high probability of brain penetration, similar to that offered by the positive control testosterone (T) (Fig. 8).

2.8. *In silico testing of compound **10** safety profile*

As compound **10** demonstrated the best pharmacological profile, we decide to assess its toxicity profile and metabolism *in silico* with Toxtree software v. 3.1.0 [78]. Compound **10** showed an acceptable safety profile (Table S2, supplementary material), no structural alerts were found for *in vitro* mutagenicity, genotoxic or non-genotoxic carcinogenicity, and no DNA binding alerts were detected. Further *in vivo* testing is needed to assess the heterocyclic rings and the hydrogen bond-accepting structure safety, which cannot permit a strong initial presumption of safety.

We additionally used the Toxtree Cytochrome P450-mediated metabolism module to predict the more plausible metabolites of compound **10** (Table S3, supplementary material). The four predicted metabolites displayed similar safety results to the parent compound (Table S4-to S6, supplementary material). Therefore, the obtained results made the molecule suitable to continue with the *in vivo* tests.

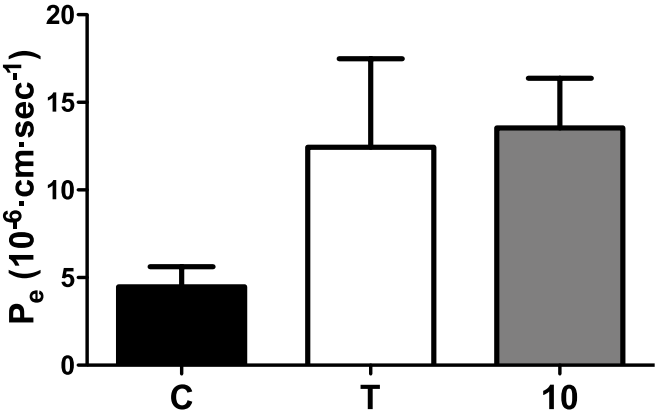

Fig. 8. Brain permeability of compound **10** evaluated by PAMPA. Permeability (Pe) is expressed as mean ± SEM of three independent assays by triplicate. Caffeine (**C**) and Testosterone (**T**) were used as internal standards [77], defining either compromised or guaranteed permeability, respectively. A value of $P_e > 5$ would indicate a high probability of blood-brain barrier crossing. (SINGLE COLUMN FITTING FIGURE).

2.9. *Compound **10** rescued the memory deficit of mice subjected to LPS in the object recognition test*

Backed by the BBB permeability data, we next performed the first *in vivo* studies with the lead compound **10**. To this end, we assessed whether this compound could abrogate the cognitive impairment in a classical *in vivo* model of neurodegeneration, *i.e.* the object recognition test in mice subjected to lipopolysaccharide (LPS) (Fig. 9). In this test, the short-term memory of mice is measured, by comparing the exploration time between an object previously shown in a training phase (see experimental part), and another one introduced in the test phase. Mice with normal short-term memory are expected to explore the novel object for a longer time compared with animals subjected to a neurotoxicant such as LPS that induced neurodegeneration and memory loss [79]. The neurodegenerative effects of LPS have been comprehensively reviewed [80], and include the development of tauopathy and reduced short-term memory [81].

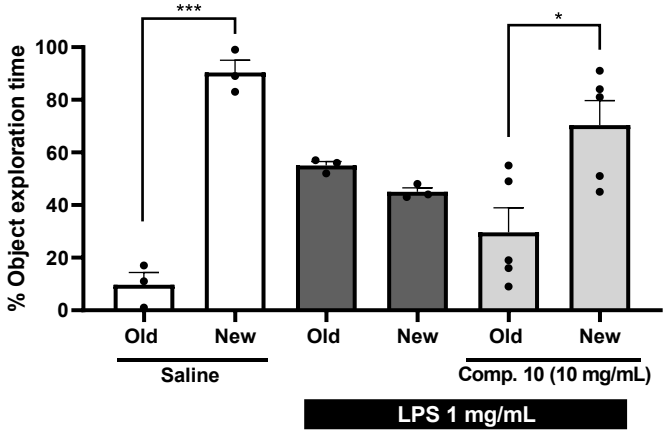

Fig. 9. Percentage of exploration time of mice submitted to the object recognition test. According to the protocol (experimental part), all mice were first familiarized with the experimental arena. In the training phase, mice were allowed to freely explore two equal objects in the box. In the test phase, one of those is replaced by a different object, and the time exploring each object is compared. The bars show the exploration times of the old *versus* the new object in untreated mice, mice treated with LPS, and mice treated with compound **10** and LPS, in the test phase. Data represent mean ± SEM of at least three independent experiments. ***$P < 0.001$, *$p < 0.05$, comparing time exploring new and old objects. (1.5 COLUMN FITTING FIGURE).

As expected, *i.p.* injection of LPS 1 mg/mL provoked mice to lose interest for the novel object, as no significant difference was observed between the exploration time of the old *versus* the new object in the test phase (Fig. 9), inferring that their memory was compromised. However, co-injection of compound **10** at a 10 mg/mL *i.p.* dose, impeded such loss of memory, as LPS-subjected mice treated with compound **10** now invested significantly more time (2.4-fold) exploring the new object *versus* the old one (Fig. 9).

3. Conclusions

In summary, the rigid analog of the OA central fragment **10**, emerged as the lead compound of a family of unsaturated *C*-glycosides with a potential profile as PADs. The restoration of inhibited PP2A phosphatase activity, sustained by *in vitro,* cellular and *in vivo* assays, reset the phosphorylation/dephosphorylation balance in cells, and elicited neuroprotection in several *in vitro* models of neurodegeneration, e.g. promoted by oxidative stress or excitotoxicity inducers. We also confirmed that compound **10** had the ability to pass through the BBB and to rescue the cognitive impairment of LPS-injected mice. Thus, our current study has clearly validated the principle of using OA as a starting point for the rational design of new drugs acting as PP2A re-activators. Since the 80*s*, OA has been the object of extensive studies by organic chemists taking it as a synthetic challenge, due to its highly complex structure. However, these contributions merely focused on reaching the final polyketide structure and, in scarce examples, probed their PP2A inhibitory action, without realizing that small fragments lacking the C1–C15 moiety might exert an allosteric activation. Recently, Aponick and co-workers described the synthesis of Spirastrellolide A analogues with high structural similarity to OA fragments [82]. Besides the extensive synthetic work, these authors reported maximal PP2A inhibitory activities of several derivatives of about 20% when tested at concentrations as high as 30 μM. However, we would hypothesize that those derivatives might actually behave as PADs at much lower concentrations under a protocol specifically designed to monitor enzymatic activators.

Overall, the therapeutic interest of PP2A activation in neurodegenerative diseases is not limited to AD, as its activity has been found compromised in vascular dementia [83], Parkinson's disease and dementia with Lewy bodies [84] and traumatic brain injury [85], among others [86–88], where several PADs have been investigated [89–92]. Future experiments are needed to deeper characterize the compound **10** as a new PAD in a pre-clinical stage, and ultimately, in clinic trials, testing its applicability to treat neurodegenerative diseases, and potentially, other PP2A signaling diseases.

4. Experimental section

4.1. Reagents and general procedures

Most of the reagents for synthesis and biological assays were purchased from Merck (Darmstadt, Germany). Sodium methoxide was obtained from Alfa Aesar (Haverhill, MA, USA). Oligomycin A and cytostatin were purchased from Santa Cruz Biotechnology (Dallas, TX, USA). Inorganic salts and solvents with analytical grade, used for reactions, work-ups and chromatographic purifications, as well as deuterated solvents for NMR, were purchased from Avantor (Radnor, PA, USA). Chlorinated solvents were neutralized before use by basic alumina 90 (Merck) to remove HCl traces. For cell culturing, minimum essential medium Eagle (MEM) and Ham's F12 nutrient were acquired from Merck. Non-essential amino acids, fetal bovine serum (FBS) that was heat-inactivated for 30 min before use, and neurobasal medium were acquired from Gibco (Madrid, Spain). BCA Protein Assay kit was purchased from Thermo Fisher Scientific (Waltham, MA, USA). Phosphatase Assay kit (*p*NPP method) was purchased from G-Biosciences (St Louis, MO, USA). The ECL Select Western Blotting Detection Reagent was supplied by GE Healthcare (Amersham, UK). Polyclonal *anti-p*-GSK-3β (Ser9) and monoclonal *anti*-GSK-3β and *anti*-β-actin (rabbit, 1:1000) were purchased from Cell Signaling Technology (Danvers, Ma, USA). Monoclonal *anti*-GFP (mouse, 1:3000) was generously donated by Dr. P. Parker (Francis Crick Institute, London, UK). The IgG-HRP (goat, mouse and rabbit, 1:5000) was purchased from Santa Cruz Biotechnology. Monoclonal *anti-p*-tau AT8 (Ser202, Thr205)(mouse, 1:1000) was purchased from Thermo Fisher Scientific. Sterile plasticware was obtained from Corning (Madrid, Spain). All reactions have been executed under Schlenk conditions, *i.e.* heating-flamed systems purged by vacuum/argon filling cycles, then reactions under argon atmosphere and the selected solvents freshly distilled. Reactions were monitored by silica gel 60 mesh on TLC foils having 254 nm fluorescent indicator and, in some cases, developed with iodine (Merck) or PMA stains (Acros Organics, Geel, Belgium). Chromatographic purifications were carried out with an automatized flash chromatography station Isolera One (Biotage, Uppsala, Sweden) using pre-charged columns ZIP, SNAP and Sfär from the same manufacturer. Mobile phases were based on hexane/ethyl acetate mixtures. Compounds were characterized by ^{1}H y^{13}C NMR spectra, acquired in a Bruker Avance 300 (Billerica, MA, USA) internally referenced with the residual signal of ^{1}H presented in the selected deuterated solvents. NMR signals are depicted according to their parts per million (ppm), coupling constants (*J*) in Hz and the relative integral. High resolution mass spectra (HRMS) were obtained under the electrospray technique in the positive mode in a VG AutoSpec Waters/QSTAR station (Applied Biosystems, Waltham, MA, USA). Melting points were obtained from a SMP-10 apparatus (Stuart, Staffordshire, UK) and are uncorrected. Optical rotary deviations ($[\alpha]_d$) of compounds were obtained at 25 °C from a polarimeter PerkinElmer 241 (Waltham, MA, USA), provided of a Na lamp (glass cell 2 × 10 cm), and calculated with the formula $[\alpha]_d = \alpha/l \times c$, where α is the specific rotation acquired, l is the cell length in dm, c is the concentration as g/mL and D is the wavelength, corresponding to 589 nm (line D of Na lamp). All compounds described and evaluated presented purity >95%, as confirmed by elemental analyses performed in a LECO CHNS-932 apparatus (analyses indicated by the symbols of the elements were within ±0.4% of the theoretical value).

4.2. Synthesis of (2R,3S,6R)-6-alyl-3,6-dihydro-2-(hydroxymethyl)-2H-pyran-3-ol (2)

To a solution of **1** [60] (2.5 g, 9.83 mmol) in MeOH (3.25 mL/mmol **1**), MeONa (2 eq, 19.66 mmol, 1.06 g) was added portion-wise, and the reaction mixture was stirred at rt for 16 h until it was completed (TLC). Solvent was evaporated and a saturated solution of NH_4Cl was poured up to mixture reached pH 7. Then, the mixture was extracted with DCM (3 × 50 mL) and the combined organic layer dried over anhydrous Na_2SO_4, filtered and the solvent evaporated, yielding **2** as a yellow oil (1.67 g, >99%) that did not require further purification, having spectral and analytical (C, H) characteristics according to the literature [93]. $[\alpha]_D = -15.5$ (*c* 1.22, DCM); lit. −23.8 (*c* 0.88, $CHCl_3$) [93].

4.3. Synthesis of (4aR,6R,8aS)-6-alyl-2-phenyl-4,4a,6,8a-tetrahydropyrane[3,2-d][1,3]dioxin (3)

To a solution of **2** (345 mg, 2.03 mmol) in 1,2-DCE (1,6 mL/mmol **2**), camphorsulfonic acid (CSA, 2 eq, 943 mg, 4,06 mmol) and dimethoxymethylbenzene (1 eq, 2.03 mmol, 305 μL) were added. Reaction was stirred at rt for 16 h, and then interrupted by addition of a saturated solution $NaHCO_3$ (20 mL). The mixture was extracted with DCM (3 × 20 mL) and the combined organic layer was dried over anhydrous Na_2SO_4, filtered and the solvent evaporated. The crude was purified by automatized flash chromatography using hexane/ethyl acetate mixtures as eluent, furnishing **3** (310 mg, 59%) as a white solid, with spectral and analytical (C, H) characteristics according to the literature [61]. Mp 60–62 °C; lit. 63 °C [61]. $[\alpha]_D = +36.0$ (*c* 1.11, DCM); lit. +26.7 (*c* 1.25, $CHCl_3$) [61].

4.4. Synthesis of (4aR,6R,8aS)-6-alyl-2,2-dimethyl-4,4a,6,8a-tetrahydropyran[3,2-d][1,3]dioxin (**4**)

Following the protocol described by Nicolau et al. [94] with slight modifications, to a solution of **2** (1.24 g, 7.29 mmol) in DCM (4 mL/mmol **2**) at 0 °C, pyridinium *p*-toluenesulfonate (0.05 eq, 0.36 mmol, 90 mg) was added. Then, 2-methoxypropene (1.5 eq, 10.93 mmol, 1.05 mL) was injected dropwise for 15 min, and the mixture stirred at 0 °C for 2 h. Then, reaction was allowed to warm up to rt and 1 eq more of 2-methoxypropene was injected (7.29 mmol, 0.7 mL), allowing 3 h more of stirring. Once completed (TLC), reaction was diluted with diethyl ether, washed with water (2 × 20 mL) and brine (20 mL), dried over $MgSO_4$, filtered and the solvent evaporated. Compound **4** was obtained as yellowish oil (1.53 g, >99%) that did not need further purification, showing spectral and analytical (C, H) characteristics according to the literature [94]. $[\alpha]_D = -25.6$ (*c* 1.06, DCM); lit. −19.9 (*c* 2.02, $CHCl_3$) [94].

4.5. General procedure for the hydroboration/oxidation reaction of **3** and **4**

To a solution of alkenes **3** or **4** (1 eq) in THF (1.35 mL/mmol), 9-BBN (0.5 M in THF, 1 eq) was added slowly, and the reaction was stirred at rt for 1 h. Then, it was cooled down to 0 °C and NaOH (3 M, 1 mL/mmol) and H_2O_2 (30% vol., 1 mL/mmol) were successively injected. When addition was completed, the mixture was allowed to warm up to rt and stirred for 30 min. Finally, the mixture was extracted with DCM (3 × 10 mL), the combined organic layer dried with anhydrous Na_2SO_4, filtered and the solvent evaporated. The crude was purified by flash chromatography or preparative TLC, using hexane/ethyl acetate mixtures as eluent.

4.5.1. 3-[(4aR,6R,8aS)-2-phenyl-4,4a,6,8a-tetrahydropyran[3,2-d][1,3]dioxin-6-yl]propan-1-ol (**5**)

According to the general method 4.5, compound **3** (421 mg, 1.63 mmol) [9-BBN (1.63 mmol, 3.26 mL), NaOH (1.6 mL), H_2O_2 (1.6 mL)] yielded, after chromatographic purification (preparative TLC), **5** as a white solid (99 mg, 22%), showing spectral and analytical (C, H) characteristics according to the literature [61]. Mp 81–83 °C; lit. 81 °C [61]. $[\alpha]_D = +15.1$ (*c* 1.00, DCM); lit. +31.0 (*c* 1.05, $CHCl_3$) [61].

4.5.2. 3-[(4aR,6R,8aS)-2,2-dimethyl-4,4a,6,8a-tetrahydropyran[3,2-d][1,3]dioxin-6-yl]propan-1-ol (**6**)

According to the general method 4.5, compound **4** (1.24 g, 5.08 mmol) [9-BBN (5.08 mmol, 10.1 mL), NaOH (5.1 mL), H_2O_2 (5.1 mL)] yielded, after chromatographic purification, **6** as a colorless oil (1.1 g, 82%), showing spectral and analytical (C, H) characteristics according to the literature [94]. $[\alpha]_D = -14.7$ (*c* 1.16, DCM); lit. −18.0 (*c* 1.20, $CHCl_3$) [94].

4.6. General procedure for the Sharpless' dihydroxylations of **3** and **4**

To a solution of **3** or **4** (1 eq) in a *t*-BuOH/H_2O (1:1) mixture (20 mL/mmol) at 0 °C, AD-mix α or β reagent (1.8 eq) was added. The reaction was stirred at 0 °C for 6 h. Once completed (TLC), it was quenched with saturated $NaHSO_3$ (10 mL). The mixture was concentrated to remove tert-butanol, and the resulting aqueous crude was extracted with ethyl acetate (3 × 10 mL). The combined organic layer was dried over anhydrous Na_2SO_4, filtered and the solvent evaporated, yielding pure compound that did not need further chromatographic purification.

4.6.1. (2R)-3-[(4aR,6R,8aS)-2-phenyl-4,4a,6,8a-tetrahydropyran[3,2-d][1,3]dioxin-6-yl]propan-1,2-diol (**7**)

According to the general method 4.6, compound **3** (89 mg, 0.34 mmol) [AD-mix-β (477 mg, 0.61 mmol)] yielded **7** as a white solid (101 mg, >99%). Mp 129–131 °C. $[\alpha]_D = +38.4$ (*c* 1.20, DCM). ^{1}H NMR (300 MHz, $CDCl_3$) δ 7.49 (m, 2H, Ar), 7.36 (m, 3H, Ar), 6.01 (m, 1H, H8), 5.70 (m, 1H, H7), 5.59 (s, 1H, H2), 4.59 (m, 1H, H6), 4.26 (dd, $J = 10.5$, 4.5 Hz, 1H, H8a), 4.15 (m, 1H, H4), 3.96 (m, 1H, H2′), 3.78 (t, $J = 10.2$ Hz, 1H, H4), 3.66 (m, 1H, H1′), 3.56 (m, 1H, H1′), 3.48 (m, 1H, H4a), 2.64 (bs, 2H, OH), 1.81 (ddd, $J = 14.7$, 11.1, 3.3 Hz, 1H, H3′), 1.60–1.47 (m, 1H, H3'). ^{13}C NMR (75.4 MHz, $CDCl_3$) δ 137.5, 130.9, 129.3, 128.5, 126.8, 126.3, 102.1,75.4, 71.1, 69.8, 69.2, 67.0, 65.3, 36.0. HRMS (ESI^+) mass calcd for $C_{16}H_{20}O_5Na$ (*m/z*) 315.1203 (M + Na^+); found, 315.1198. Anal. $C_{16}H_{20}O_5$ (C, H).

4.6.2. (2R)-3-[(4aR,6R,8aS)-2,2-dimethyl-4,4a,6,8a-tetrahydropyran[3,2-d][1,3]dioxin-6-yl]propan-1,2-diol (**8**)

According to the general method 4.6, compound **4** (80 mg, 0.38 mmol) [AD-mix-β (534 mg, 0.68 mmol)] yielded **8** as a yellowish oil (80 mg, 82%). $[\alpha]_D = -13.7$ (*c* 1.10, DCM). ^{1}H NMR (300 MHz, $CDCl_3$) δ 5.81 (m, 1H, H8), 5.63 (m, 1H, H7), 4.50 (m, 1H, H6), 4.17 (m, 1H, H8a), 3.94–3.78 (m, 2H, H2′, H4), 3.72 (t, $J = 9.0$ Hz, 1H, H4), 3.59 (dd, $J = 11.2$, 3.2 Hz, 1H, H1′), 3.46–3.27 (m, 2H, H1′, H4a), 3.25 (bs, 2H, OH), 1.79–1.63 (m, 1H, H3′), 1.49 (s, 3H, CH_3), 1.46 (m, 1H, H3'), 1.40 (s, 3H, CH_3). ^{13}C NMR (75.4 MHz, $CDCl_3$) δ 130.7, 127.4, 99.9, 70.9, 69.1, 67.7, 67.0, 66.3, 63.3, 36.1, 29.3, 19.1. HRMS (ESI^+) mass calcd for $C_{12}H_{20}O_5Na$ (*m/z*) 267.1203 (M + Na^+); found, 267.1203. Anal. $C_{12}H_{20}O_5$ (C, H).

4.6.3. (2S)-3-[(4aR,6R,8aS)-2-phenyl-4,4a,6,8a-tetrahydropyran[3,2-d][1,3]dioxin-6-yl]propan-1,2-diol (**9**)

According to the general method 4.6, compound **3** (120 mg, 0.46 mmol) [AD-mix-α (645 mg, 0.83 mmol)] yielded **9** as a white solid (112 mg, 82%). Mp 120–122 °C. $[\alpha]_D = +50.4$ (*c* 1.11, DCM). ^{1}H NMR (300 MHz, $CDCl_3$) δ 7.52–7.46 (m, 2H, Ar), 7.40–7.34 (m, 3H, Ar), 6.00 (m, 1H, H8), 5,69 (m, 1H, H7), 5.58 (s, 1H, H2), 4.53 (m, 1H, H6), 4.26 (dd, $J = 10.2$, 4.5 Hz, 1H, H8a), 4.15 (bd, $J = 8.1$ Hz, 1H, H4), 3.94 (m, 1H, H2′), 3.77 (t, $J = 10.2$ Hz, 1H, H4), 3.67–3.57 (m, 2H, H1′), 3.56–3.45 (m, 1H, H4a), 2.90 (bs, 2H, OH), 2.00–1.84 (m, 1H, H3′), 1.70–1.57 (m, 1H, H3'). ^{13}C NMR (75.4 MHz, $CDCl_3$) δ 137.4, 130.1, 129.3, 128.5, 127.1, 126.3, 102.1, 75.0, 74.0, 71.6, 69.5, 66.3, 65.4, 35.7. HRMS (ESI^+) mass calcd for $C_{16}H_{20}O_5Na$ (*m/z*) 315.1203 (M + Na^+); found, 315.1204. Anal. $C_{16}H_{20}O_5$ (C, H).

4.6.4. (2S)-3-[(4aR,6R,8aS)-2,2-dimethyl-4,4a,6,8a-tetrahydropyran[3,2-d][1,3]dioxin-6-yl]propan-1,2-diol (**10**)

According to the general method 4.6, compound **4** (95 mg, 0.45 mmol) [AD-mix-α (631 mg, 0.81 mmol)] yielded **10** as a yellowish oil (73 mg, 63%). $[\alpha]_D = +16.5$ (*c* 1.01, DCM). ^{1}H NMR (300 MHz, $CDCl_3$) δ 5.83 (m, 1H, H8), 5.63 (dt, $J = 10.5$, 2.4 Hz, 1H, H7), 4.49 (m, 1H, H6), 4.18 (bd, $J = 8.1$ Hz, 1H, H8a), 3.92 (m, 1H, H2′), 3.84 (dd, $J = 10.5$, 5.1 Hz, 1H, H4), 3.74 (t, $J = 10.5$ Hz, 1H, H4), 3.61 (ddd, $J = 11.1$, 3.6, 0.6 Hz, 1H, H1′), 3.55–3.38 (m, 2H, H1′, H4a), 3.10 (bs, 2H, OH), 1.98–1.83 (m, 1H, H3′), 1.59 (dt, $J = 14.7$, 3.3 Hz, 1H, H3'), 1.50 (s, 3H, CH_3), 1.42 (s, 3H, CH_3). ^{13}C NMR (75.4 MHz, $CDCl_3$) δ 129.8, 127.9, 100.0, 74.2, 71.7, 67.4, 66.5, 66.4, 63.2, 35.8, 29.3, 19.1. HRMS (ESI^+) mass calcd for $C_{12}H_{20}O_5Na$ (*m/z*) 267.1203 (M + Na^+); found, 267.1201. Anal. $C_{12}H_{20}O_5$ (C,H).

4.7. General procedure for the benzoylation of **5** and **6**

To a solution of **5** or **6** (1 eq) in pyridine (3 mL/mmol), benzoyl chloride (1.1 eq) was added dropwise at rt. The reaction was stirred for 18 h and then interrupted by dilution with 10 mL of $CHCl_3$. The mixture was washed with water (10 mL) and NH_4Cl (2 × 10 mL), and the organic layer dried over anhydrous Na_2SO_4, filtered, and evaporated. The crude was purified by automatized flash chromatography using hexane/ethyl acetate mixtures as eluent.

4.7.1. 3-[(4aR,6R,8aS)-2-phenyl-4,4a,6,8a-tetrahydropyran[3,2-d][1,3]dioxin-6-yl]propyl benzoate (11)

According to the general method 4.7, compound **5** (94 mg, 0.34 mmol) [benzoyl chloride (0.37 mmol, 43 μL)] yielded, after chromatographic purification, **11** as a white solid (19 mg, 15%), showing spectral and analytical (C, H) characteristics according to the literature [61]. Mp 86–88 °C; lit. 84 °C [61]. $[\alpha]_D = +10.0$ (*c* 0.99, DCM); lit. +11.7 (*c* 1.58, $CHCl_3$) [61].

4.7.2. 3-[(4aR,6R,8aS)-2,2-dimethyl-4,4a,6,8a-tetrahydropyran[3,2-d][1,3]dioxin-6-yl]propyl benzoate (12)

According to the general method 4.7, compound **6** (60 mg, 0.26 mmol) [benzoyl chloride (0.28 mmol, 33 μL)] yielded, after chromatographic purification, **12** as a white solid (7 mg, 8%). Mp 80–84 °C. $[\alpha]_D = -21.0$ (*c* 1.00, DCM). ^{1}H NMR (300 MHz, $CDCl_3$) δ 8.04 (d, $J = 7.8$ Hz, 2H, Ar), 7.56 (m, 1H, Ar), 7.44 (m, 2H, Ar), 5.85 (bd, $J = 10.5$ Hz, 1H, H8), 5.70 (dt, $J = 10.5$, 2.4 Hz, 1H, H7), 4.36 (m, 2H, H1′), 4.26 (m, 1H, H6), 4.20 (d, $J = 8.7$ Hz, 1H, H8a), 3.89 (dd, $J = 10.5$, 5.1 Hz, 1H, H4), 3.76 (t, $J = 10.5$ Hz, 1H, H4), 3.41 (ddd, $J = 10.2$, 8.7, 5.1 Hz, 1H, H4a), 2.04–1.76 (m, 3H, H2′, H3′), 1.71–1.50 (m, 1H, H3'), 1.53 (s, 1H, CH_3), 1.44 (s, 1H, CH_3). ^{13}C NMR (75.4 MHz, $CDCl_3$) δ 166.8, 133.1, 131.0, 130.4, 129.7, 128.5, 100.1, 73.3, 72.2, 64.8, 64.3, 63.1, 31.1, 29.6, 25.8. HRMS (ESI^+) mass calcd for $C_{19}H_{24}O_5Na$ (*m/z*) 355.1516 ($M + Na^+$); found, 355.1520. Anal. $C_{19}H_{24}O_5$ (C, H).

4.8. Synthesis of 3-[(2R,5S,6R)-5,6-dihydro-5-hydroxy-6-(hydroxymethyl)-2H-pyran-2-yl]propyl benzoate (13)

To solution of **6** (109 mg, 0.48 mmol) in DCM (2 mL), K_2CO_3 (2.5 eq, 1.2 mmol, 165 mmol) and benzoyl chloride (1.1. eq, 0.53 mmol, 61 μL) were added. The reaction was stirred at rt for 18 h and then interrupted by addition of 2 mL of water. The mixture was extracted with DCM (3 × 10 mL), and the combined organic layer was dried over anhydrous Na_2SO_4, filtered, and evaporated. The crude was purified by automatized flash chromatography using hexane/ethyl acetate mixtures as eluent, yielding **13** as a white solid (37 mg, 26%), showing spectral and analytical (C, H) characteristics according to the literature [61]. Mp 96–98 °C; lit. 99 °C [61]. $[\alpha]_D = -15.0$ (*c* 1.11, DCM); lit. −23.5 (*c* 1.04, $CHCl_3$) [61].

4.9. Experimental use of animals

Animals used for experimentation were bred in cages within the animal house of the School of Medicine at Universidad Autónoma de Madrid (UAM), under adequate temperature and lighting. Animals were provided water and food *ad libitum*. Maintenance and use of animals fulfilled the ethical guidelines according to the EU Council Directive (2010/63/EU) and the Spanish laws (RD 1201/2005 and 53/2013). Experiments were approved by the Ethics Committee of the UAM. Maximal effort has been made to avoid suffering to animals and reduce the number of animals sacrificed, according to the journal's guidelines, thus, animal studies were limited to validate the best compound of the family, with demonstrated interest on preceding *in vitro* work, and were therefore not used as for general screening purposes.

4.10. Cell cultures

SH-SY5Y neuroblastoma and human embryonic kidney HEK293T cell lines were acquired from American Type Culture Collection (ATCC, Manassas, VA, USA). SH-SY5Y cells were cultured in a 1:1 mixture of MEM and F12 enriched with FBS 10% and supplemented with a penicillin/streptomycin cocktail (100 UI/mL and 100 μg/mL, respectively), non-essential amino acids (0.1 mM), $NaHCO_3$ (23 mM) and sodium pyruvate (1 mM). HEK-293T cells were maintained in DMEM supplemented with 10% FBS. Cell lines were maintained in an incubator at 37 °C under moistened air atmosphere with 5% CO_2 and used in a low cell passage (8–20).

Rat cortical neuron cultures were obtained from 18 to 19 days-old embryos of pregnant rats, which were decapitated, and brains extracted. After removing meninges, the brain cortex was dissected and submerged in PBS buffer composed of (mM): NaCl 137, KCl 3, Na_2HPO_4 10, KH_2PO_4 2, bovine serum albumin (BSA) and glucose 1.5; pH 7.4. All cortices were collected and mechanically disaggregated, and cells were seeded according to a protocol previously described [95]. The number of cells was counted by Trypan Blue.

4.11. pNPP and MTT assays

SH-SY5Y cells were seeded in 48-well plates at 70000 cells/well density. The phosphatase activity of cells was measured by the *p*NPP method and the ability of compounds to protect cells against OA, cytostatin and the R/O cocktail, as well as their *per se* toxicity, were measured by the MTT reduction method, according to what has recently been described [55]. For the evaluation of neuroprotection against glutamate excitotoxicity and *per se* toxicity by compounds, rat cortical embryonic neurons were seeded in 48-well plates at 40000 cells/well density and subjected to the MTT reduction method according to what has recently been described [95].

4.12. PP2A activity experiments and protein expression determination by western-blot

PP2A activity was probed by the Malachite green method on the K-R-*p*T-I-R-R phosphopeptide (Synpeptide) using PP2A isoforms immunoprecipitated by GFP pull-down (GFP-trapping beads®, ChromoTek), according to what has recently been described [60]. Western-blot analyses of PP2A phosphoprotein substrates were conducted similarly to what has recently been described [55].

4.13. Computational docking

Compound **10** 3D conformation was generated with Spartan 20 software (Wavefunction, Inc.; Irvine, CA, USA), optimized by the *ab initio* base 6-31G* based on the Hartree-Fock method. The ligand was docked into the PP2A-AC dimer, deposited in the protein data bank (www.rcsb.com) with the PDB ID: 2IE4 [57], after removal of the co-crystalized OA and water molecules. Docking was performed using Molegro Virtual docker 3.2.1. and represented using its viewing tools. Pose selected for compound **10** was the best ranked in the MolDock Score algorithm [96].

4.14. Estimation of brain permeability by PAMPA

PAMPA allows to estimate the passive diffusion of potential CNS drugs through the BBB [77]. It was conducted and obtained P_e by a procedure recently described [97], with slight modifications. Measurements of absorbance of the acceptor (both initial and final) and donor plates, necessary for calculating compound concentrations at both sides of the artificial membrane, were acquired in a spectrophotometric reader Shimadzu UV2401PC, capable of detecting UV bands up to 200 nm, using quartz cuvettes with 1 cm path length. Caffeine (C) and testosterone (T) were used as standards to define low and high rates of passive brain diffusion [77].

4.15. New object recognition test

This test comprises three stages executed on consecutive days. First, mice were introduced into the test cage for 10 min for them to familiarize themselves with the habitat. On the second day, two equal objects were put in the cage at a certain place and distance between them, allowing mice to freely explore them. Finally, on the third day, keeping place and distance, one of the objects was replaced by one different in

shape and size. Exploratory movements of mice in the cage were recorded for 10 min. Recordings were analyzed with the Fiji program under the *MouBeat* extension. Time exploring each object was registered as a percentage of object exploration time, according to the formula:

$$\%\ Object\ exploration\ time = \frac{Time\ (s)}{Time\ new\ (s) + Time\ old\ (s)} \times 100$$

4.16. Data analysis

Statistically significant differences between testing groups were analyzed by one tail Student's t-test or one-way analysis of variance, followed by Newman-Keuls post hoc test., using GraphPad Prism 5.0 software for Mac OS X, and considering statistical difference when $p < 0.05$.

Declaration of competing interest

The authors declare that they have no known competing financial interests or personal relationships that could have appeared to influence the work reported in this paper.

Data availability

DOI: 10.17632/kv9vr2jxbm.1

Acknowledgements

This work was supported by Proyectos de Investigación en Salud (PI16/01041 and PI19/01724, IS Carlos III to CdlR, co-funded by FEDER, Spain). RLA thanks Universidad Autónoma de Madrid (UAM) for predoctoral contract. LV thanks IS Carlos III for predoctoral contract. IB thanks Fundación Teófilo Hernando (FTH) for predoctoral fellowship. MM thanks Ministerio de Educación (Spain) for Master degree fellowship.

Appendix A. Supplementary data

Supplementary data to this article can be found online at https://doi.org/10.1016/j.ejmech.2023.115245.

References

[1] S. Reynhout, V. Janssens, Physiologic functions of PP2A: lessons from genetically modified mice, Biochim. Biophys. Acta Mol. Cell Res. 1866 (2019) 31–50, https://doi.org/10.1016/j.bbamcr.2018.07.010.
[2] D.L. Brautigan, S. Shenolikar, Protein serine/threonine phosphatases: keys to unlocking regulators and substrates, Annu. Rev. Biochem. 87 (2018) 921–964, https://doi.org/10.1146/annurev-biochem-062917-012332.
[3] A.L. Jeong, Y. Yang, PP2A function toward mitotic kinases and substrates during the cell cycle, BMB Rep 46 (2013) 289–294, https://doi.org/10.5483/bmbrep.2013.46.6.041.
[4] V. Janssens, A. Rebollo, The role and therapeutic potential of Ser/Thr phosphatase PP2A in apoptotic signalling networks in human cancer cells, Curr. Mol. Med. 12 (2012) 268–287, https://doi.org/10.2174/156652412799218930.
[5] G. Nadel, Z. Yao, E. Wainstein, I. Cohen, I. Ben-Ami, A. Schajnovitz, G. Maik-Rachline, Z. Naor, B.A. Horwitz, R. Seger, GqPCR-stimulated dephosphorylation of AKT is induced by an IGBP1-mediated PP2A switch, Cell Commun. Signal. 20 (2022) 5, https://doi.org/10.1186/s12964-021-00805-z.
[6] E. Ferrari, C. Bruhn, M. Peretti, C. Cassani, W.V. Carotenuto, M. Elgendy, G. Shubassi, C. Lucca, R. Bermejo, M. Varasi, S. Minucci, M.P. Longhese, M. Foiani, PP2A controls genome integrity by integrating nutrient-sensing and metabolic pathways with the DNA damage response, Mol. Cell. 67 (2017) 266–281 e264, https://doi.org/10.1016/j.molcel.2017.05.027.
[7] K. Heo, H. Basu, A. Gutnick, W. Wei, E. Shlevkov, T.L. Schwarz, Serine/threonine protein phosphatase 2A regulates the transport of axonal mitochondria, Front. Cell. Neurosci. 16 (2022), 852245, https://doi.org/10.3389/fncel.2022.852245.
[8] P. Seshacharyulu, P. Pandey, K. Datta, S.K. Batra, Phosphatase: PP2A structural importance, regulation and its aberrant expression in cancer, Cancer Lett. 335 (2013) 9–18, https://doi.org/10.1016/j.canlet.2013.02.036.
[9] C. Lambrecht, D. Haesen, W. Sents, E. Ivanova, V. Janssens, Structure, regulation, and pharmacological modulation of PP2A phosphatases, Methods Mol. Biol. 1053 (2013) 283–305, https://doi.org/10.1007/978-1-62703-562-0_17.
[10] V. Janssens, S. Longin, J. Goris, PP2A holoenzyme assembly: in cauda venenum (the sting is in the tail), Trends Biochem. Sci. 33 (2008) 113–121, https://doi.org/10.1016/j.tibs.2007.12.004.
[11] R. Yabe, S. Tsuji, S. Mochida, T. Ikehara, T. Usui, T. Ohama, K. Sato, A stable association with PME-1 may be dispensable for PP2A demethylation - implications for the detection of PP2A methylation and immunoprecipitation, FEBS Open Bio. 8 (2018) 1486–1496, https://doi.org/10.1002/2211-5463.12485.
[12] J.M. Sontag, D. Schuhmacher, G. Taleski, A. Jordan, S. Khan, A. Hoffman, R. J. Gomez, M.D. Mazalouskas, S.K. Hanks, B.W. Spiller, E. Sontag, B.E. Wadzinski, A new paradigm for regulation of protein phosphatase 2A function via Src and Fyn kinase-mediated tyrosine phosphorylation, J. Biol. Chem. 298 (2022), 102248, https://doi.org/10.1016/j.jbc.2022.102248.
[13] D. Haesen, W. Sents, E. Ivanova, C. Lambrecht, V. Janssens, Cellular inhibitors of protein phosphatase PP2A in cancer, Biomed. Res. 23 (2012) 197–211.
[14] E.C. Dacol, S. Wang, Y. Chen, A.P. Lepique, The interaction of SET and protein phosphatase 2A as target for cancer therapy, Biochim. Biophys. Acta Rev. Canc 1876 (2021), 188578, https://doi.org/10.1016/j.bbcan.2021.188578.
[15] Y.P. Shentu, Y. Huo, X.L. Feng, J. Gilbert, Q. Zhang, Z.Y. Liuyang, X.L. Wang, G. Wang, H. Zhou, X.C. Wang, J.Z. Wang, Y.M. Lu, J. Westermarck, H.Y. Man, R. Liu, CIP2A causes tau/APP phosphorylation, synaptopathy, and memory deficits in alzheimer's disease, Cell Rep. 24 (2018) 713–723, https://doi.org/10.1016/j.celrep.2018.06.009.
[16] O. Kauko, S.Y. Imanishi, E. Kulesskiy, L. Yetukuri, T.D. Laajala, M. Sharma, K. Pavic, A. Aakula, C. Rupp, M. Jumppanen, P. Haapaniemi, L. Ruan, B. Yadav, V. Suni, T. Varila, G.L. Corthals, J. Reimand, K. Wennerberg, T. Aittokallio, J. Westermarck, Phosphoproteome and drug-response effects mediated by the three protein phosphatase 2A inhibitor proteins CIP2A, SET, and PME-1, J. Biol. Chem. 295 (2020) 4194–4211, https://doi.org/10.1074/jbc.RA119.011265.
[17] C.M. O'Connor, A. Perl, D. Leonard, J. Sangodkar, G. Narla, Therapeutic targeting of PP2A, Int. J. Biochem. Cell Biol. 96 (2018) 182–193, https://doi.org/10.1016/j.biocel.2017.10.008.
[18] R. Lajarin-Cuesta, R.L. Arribas, C. De Los Rios, Ligands for Ser/Thr phosphoprotein phosphatases: a patent review (2005-2015), Expert Opin. Ther. Pat. 26 (2016) 389–407, https://doi.org/10.1517/13543776.2016.1135903.
[19] J. Sangodkar, A. Perl, R. Tohme, J. Kiselar, D.B. Kastrinsky, N. Zaware, S. Izadmehr, S. Mazhar, D.D. Wiredja, C.M. O'Connor, D. Hoon, N.S. Dhawan, D. Schlatzer, S. Yao, D. Leonard, A.C. Borczuk, G. Gokulrangan, L. Wang, E. Svenson, C.C. Farrington, E. Yuan, R.A. Avelar, A. Stachnik, B. Smith, V. Gidwani, H.M. Giannini, D. McQuaid, K. McClinch, Z. Wang, A.C. Levine, R. C. Sears, E.Y. Chen, Q. Duan, M. Datt, S. Haider, A. Ma'ayan, A. DiFeo, N. Sharma, M.D. Galsky, D.L. Brautigan, Y.A. Ioannou, W. Xu, M.R. Chance, M. Ohlmeyer, G. Narla, Activation of tumor suppressor protein PP2A inhibits KRAS-driven tumor growth, J. Clin. Invest. 127 (2017) 2081–2090, https://doi.org/10.1172/JCI89548.
[20] C.C. Farrington, E. Yuan, S. Mazhar, S. Izadmehr, L. Hurst, B.L. Allen-Petersen, M. Janghorban, E. Chung, G. Wolczanski, M. Galsky, R. Sears, J. Sangodkar, G. Narla, Protein phosphatase 2A activation as a therapeutic strategy for managing MYC-driven cancers, J. Biol. Chem. 295 (2020) 757–770, https://doi.org/10.1074/jbc.RA119.011443.
[21] B. Meeusen, E.E. Cortesi, J. Domenech Omella, A. Sablina, J.J. Ventura, V. Janssens, PPP2R4 dysfunction promotes KRAS-mutant lung adenocarcinoma development and mediates opposite responses to MEK and mTOR inhibition, Cancer Lett. 520 (2021) 57–67, https://doi.org/10.1016/j.canlet.2021.06.022.
[22] Y.T. Yen, M. Chien, P.Y. Wu, C.C. Ho, C.T. Ho, K.C. Huang, S.F. Chiang, K.S. C. Chao, W.T. Chen, S.C. Hung, Protein phosphatase 2A inactivation induces microsatellite instability, neoantigen production and immune response, Nat. Commun. 12 (2021) 7297, https://doi.org/10.1038/s41467-021-27620-x.
[23] A. Laine, S.G. Nagelli, C. Farrington, U. Butt, A.N. Cvrljevic, J.P. Vainonen, F. M. Feringa, T.J. Gronroos, P. Gautam, S. Khan, H. Sihto, X. Qiao, K. Pavic, D. C. Connolly, P. Kronqvist, L.L. Elo, J. Maurer, K. Wennerberg, R.H. Medema, H. Joensuu, E. Peuhu, K. de Visser, G. Narla, J. Westermarck, CIP2A interacts with TopBP1 and drives basal-like breast cancer tumorigenesis, Cancer Res. 81 (2021) 4319–4331, https://doi.org/10.1158/0008-5472.CAN-20-3651.
[24] M.P. Ward, J.P. Spiers, Protein phosphatase 2A regulation of markers of extracellular matrix remodelling in hepatocellular carcinoma cells: functional consequences for tumour invasion, Br. J. Pharmacol. 174 (2017) 1116–1130, https://doi.org/10.1111/bph.13759.
[25] D. Haesen, W. Sents, K. Lemaire, Y. Hoorne, V. Janssens, The basic biology of PP2A in hematologic cells and malignancies, Front. Oncol. 4 (2014) 347, https://doi.org/10.3389/fonc.2014.00347.
[26] M.D. Dun, A. Mannan, C.J. Rigby, S. Butler, H.D. Toop, D. Beck, P. Connerty, J. Sillar, R.G.S. Kahl, R.J. Duchatel, Z. Germon, S. Faulkner, M. Chi, D. Skerrett-Byrne, H.C. Murray, H. Flanagan, J.G. Almazi, H. Hondermarck, B. Nixon, G. De Iuliis, J. Chamberlain, F. Alvaro, C.E. de Bock, J.C. Morris, A.K. Enjeti, N. M. Verrills, Shwachman-Bodian-Diamond syndrome (SBDS) protein is a direct inhibitor of protein phosphatase 2A (PP2A) activity and overexpressed in acute myeloid leukaemia, Leukemia 34 (2020) 3393–3397, https://doi.org/10.1038/s41375-020-0814-0.
[27] F. Liu, I. Grundke-Iqbal, K. Iqbal, C.X. Gong, Contributions of protein phosphatases PP1, PP2A, PP2B and PP5 to the regulation of tau phosphorylation, Eur. J. Neurosci. 22 (2005) 1942–1950, https://doi.org/10.1111/j.1460-9568.2005.04391.x.
[28] G. Taleski, E. Sontag, Protein phosphatase 2A and tau: an orchestrated 'Pas de Deux, FEBS Lett. 592 (2018) 1079–1095, https://doi.org/10.1002/1873-3468.12907.

[29] I. Grundke-Iqbal, K. Iqbal, Y.C. Tung, M. Quinlan, H.M. Wisniewski, L.I. Binder, Abnormal phosphorylation of the microtubule-associated protein tau (tau) in Alzheimer cytoskeletal pathology, Proc. Natl. Acad. Sci. U. S. A. 83 (1986) 4913–4917, https://doi.org/10.1073/pnas.83.13.4913.
[30] S. Kins, P. Kurosinski, R.M. Nitsch, J. Gotz, Activation of the ERK and JNK signaling pathways caused by neuron-specific inhibition of PP2A in transgenic mice, Am. J. Pathol. 163 (2003) 833–843, https://doi.org/10.1016/S0002-9440(10)63444-X.
[31] J.V. Louis, E. Martens, P. Borghgraef, C. Lambrecht, W. Sents, S. Longin, K. Zwaenepoel, R. Pijnenborg, I. Landrieu, G. Lippens, B. Ledermann, J. Gotz, F. Van Leuven, J. Goris, V. Janssens, Mice lacking phosphatase PP2A subunit PR61/B'delta (Ppp2r5d) develop spatially restricted tauopathy by deregulation of CDK5 and GSK3beta, Proc. Natl. Acad. Sci. U. S. A. 108 (2011) 6957–6962, https://doi.org/10.1073/pnas.1018777108.
[32] E. Sontag, V. Nunbhakdi-Craig, J.M. Sontag, R. Diaz-Arrastia, E. Ogris, S. Dayal, S. R. Lentz, E. Arning, T. Bottiglieri, Protein phosphatase 2A methyltransferase links homocysteine metabolism with tau and amyloid precursor protein regulation, J. Neurosci. 27 (2007) 2751–2759, https://doi.org/10.1523/JNEUROSCI.3316-06.2007.
[33] C.M. O'Connor, M.T. Hoffa, S.E. Taylor, R.A. Avelar, G. Narla, Protein phosphatase 2A Aalpha regulates Abeta protein expression and stability, J. Biol. Chem. 294 (2019) 5923–5934, https://doi.org/10.1074/jbc.RA119.007593.
[34] B. Zhao, L. Sun, M. Haas, A.G. Denenberg, H.R. Wong, T.P. Shanley, PP2A regulates upstream members of the c-jun N-terminal kinase mitogen-activated protein kinase signaling pathway, Shock 29 (2008) 181–188, https://doi.org/10.1097/SHK.0b013e318070c840.
[35] D.M. Hollenstein, G. Gerecova, N. Romanov, J. Ferrari, J. Veis, M. Janschitz, R. Beyer, C. Schuller, E. Ogris, M. Hartl, G. Ammerer, W. Reiter, A phosphatase-centric mechanism drives stress signaling response, EMBO Rep. 22 (2021), e52476, https://doi.org/10.15252/embr.202152476.
[36] M. Nematullah, M.N. Hoda, S. Nimker, F. Khan, Restoration of PP2A levels in inflamed microglial cells: important for neuroprotective M2 microglial viability, Toxicol. Appl. Pharmacol. 409 (2020), 115294, https://doi.org/10.1016/j.taap.2020.115294.
[37] T. Etelainen, V. Kulmala, R. Svarcbahs, M. Jantti, T.T. Myohanen, Prolyl oligopeptidase inhibition reduces oxidative stress via reducing NADPH oxidase activity by activating protein phosphatase 2A, Free Radic. Biol. Med. 169 (2021) 14–23, https://doi.org/10.1016/j.freeradbiomed.2021.04.001.
[38] C.E. Le Pichon, W.J. Meilandt, S. Dominguez, H. Solanoy, H. Lin, H. Ngu, A. Gogineni, A. Sengupta Ghosh, Z. Jiang, S.H. Lee, J. Maloney, V.D. Gandham, C. D. Pozniak, B. Wang, S. Lee, M. Siu, S. Patel, Z. Modrusan, X. Liu, Y. Rudhard, M. Baca, A. Gustafson, J. Kaminker, R.A.D. Carano, E.J. Huang, O. Foreman, R. Weimer, K. Scearce-Levie, J.W. Lewcock, Loss of dual leucine zipper kinase signaling is protective in animal models of neurodegenerative disease, Sci. Transl. Med. 9 (2017), https://doi.org/10.1126/scitranslmed.aag0394.
[39] M. Hayne, A. DiAntonio, Protein phosphatase 2A restrains DLK signaling to promote proper Drosophila synaptic development and mammalian cortical neuron survival, Neurobiol. Dis. 163 (2022), 105586, https://doi.org/10.1016/j.nbd.2021.105586.
[40] J.M. Sontag, E. Sontag, Protein phosphatase 2A dysfunction in Alzheimer's disease, Front. Mol. Neurosci. 7 (2014) 16, https://doi.org/10.3389/fnmol.2014.00016.
[41] R. Baskaran, B.K. Velmurugan, Protein phosphatase 2A as therapeutic targets in various disease models, Life Sci. 210 (2018) 40–46, https://doi.org/10.1016/j.lfs.2018.08.063.
[42] R.M. De Palma, S.R. Parnham, Y. Li, J.J. Oaks, Y.K. Peterson, Z.M. Szulc, B. M. Roth, Y. Xing, B. Ogretmen, The NMR-based characterization of the FTY720-SET complex reveals an alternative mechanism for the attenuation of the inhibitory SET-PP2A interaction, Faseb. J. 33 (2019) 7647–7666, https://doi.org/10.1096/fj.201802264R.
[43] Y. Zhou, D. Yang, H. Chen, C. Zheng, H. Jiang, X. Liu, X. Huang, S. Ye, S. Song, N. Jiang, Z. Zhao, S. Ma, J. Ma, K. Huang, C. Chen, X. Fan, Y. Gong, X. Wang, J. Fan, R. Liu, Y. Shentu, Polyphyllin I attenuates cognitive impairments and reduces AD-like pathology through CIP2A-PP2A signaling pathway in 3XTg-AD mice, Faseb. J. 34 (2020) 16414–16431, https://doi.org/10.1096/fj.202001499R.
[44] K.W. Lee, J.Y. Im, J.M. Woo, H. Grosso, Y.S. Kim, A.C. Cristovao, P.K. Sonsalla, D. S. Schuster, M.M. Jalbut, J.R. Fernandez, M. Voronkov, E. Junn, S.P. Braithwaite, J. B. Stock, M.M. Mouradian, Neuroprotective and anti-inflammatory properties of a coffee component in the MPTP model of Parkinson's disease, Neurotherapeutics 10 (2013) 143–153, https://doi.org/10.1007/s13311-012-0165-2.
[45] G.B. Xu, P.P. Guan, P. Wang, Prostaglandin A1 decreases the phosphorylation of tau by activating protein phosphatase 2A via a michael addition mechanism at cysteine 377, Mol. Neurobiol. 58 (2021) 1114–1127, https://doi.org/10.1007/s12035-020-02174-z.
[46] H. Wei, H.L. Zhang, X.C. Wang, J.Z. Xie, D.D. An, L. Wan, J.Z. Wang, Y. Zeng, X. J. Shu, J. Westermarck, Y.M. Lu, M. Ohlmeyer, R. Liu, Direct activation of protein phosphatase 2A (PP2A) by tricyclic sulfonamides ameliorates alzheimer's disease pathogenesis in cell and animal models, Neurotherapeutics 17 (2020) 1087–1103, https://doi.org/10.1007/s13311-020-00841-6.
[47] D. Leonard, W. Huang, S. Izadmehr, C.M. O'Connor, D.D. Wiredja, Z. Wang, N. Zaware, Y. Chen, D.M. Schlatzer, J. Kiselar, N. Vasireddi, S. Schuchner, A. L. Perl, M.D. Galsky, W. Xu, D.L. Brautigan, E. Ogris, D.J. Taylor, G. Narla, Selective PP2A enhancement through biased heterotrimer stabilization, Cell 181 (2020) 688–701 e616, https://doi.org/10.1016/j.cell.2020.03.038.
[48] C. Yang, X. Li, W. Gao, Q. Wang, L. Zhang, Y. Li, L. Li, L. Zhang, Cornel iridoid glycoside inhibits tau hyperphosphorylation via regulating cross-talk between GSK-3beta and PP2A signaling, Front. Pharmacol. 9 (2018) 682, https://doi.org/10.3389/fphar.2018.00682.
[49] K. Zeng, M. Li, J. Hu, Y.A.R. Mahaman, J. Bao, F. Huang, Y. Xia, X. Liu, Q. Wang, J. Z. Wang, Y. Yang, R. Liu, X. Wang, Ginkgo biloba extract EGb761 attenuates hyperhomocysteinemia-induced AD like tau hyperphosphorylation and cognitive impairment in rats, Curr. Alzheimer Res. 15 (2018) 89–99, https://doi.org/10.2174/1567205014666170829102135.
[50] J. Chu, J. Wang, L. Cui, S. Liu, N. An, J. Han, X. Che, C. Wu, J. Yang, Pseudoginsenoside-F11 ameliorates okadiac acid-induced learning and memory impairment in rats via modulating protein phosphatase 2A, Mech. Ageing Dev. 197 (2021), 111496, https://doi.org/10.1016/j.mad.2021.111496.
[51] C.B. Malpas, L. Vivash, S. Genc, M.M. Saling, P. Desmond, C. Steward, R.J. Hicks, J. Callahan, A. Brodtmann, S. Collins, S. Macfarlane, N.M. Corcoran, C.M. Hovens, D. Velakoulis, T.J. O'Brien, A phase IIa randomized control trial of VEL015 (sodium selenate) in mild-moderate alzheimer's disease, J. Alzheimers Dis. 54 (2016) 223–232, https://doi.org/10.3233/JAD-160544.
[52] C. de Los Rios, J. Egea, J. Marco-Contelles, R. Leon, A. Samadi, I. Iriepa, I. Moraleda, E. Galvez, A.G. Garcia, M.G. Lopez, M. Villarroya, A. Romero, Synthesis, inhibitory activity of cholinesterases, and neuroprotective profile of novel 1,8-naphthyridine derivatives, J. Med. Chem. 53 (2010) 5129–5143, https://doi.org/10.1021/jm901902w.
[53] S. Lorrio, A. Romero, L. Gonzalez-Lafuente, R. Lajarin-Cuesta, F.J. Martinez-Sanz, M. Estrada, A. Samadi, J. Marco-Contelles, M.I. Rodriguez-Franco, M. Villarroya, M.G. Lopez, C. de los Rios, PP2A ligand ITH12246 protects against memory impairment and focal cerebral ischemia in mice, ACS Chem. Neurosci. 4 (2013) 1267–1277, https://doi.org/10.1021/cn400050p.
[54] R. Lajarin-Cuesta, C. Nanclares, J.A. Arranz-Tagarro, L. Gonzalez-Lafuente, R. L. Arribas, M. Araujo de Brito, L. Gandia, C. de Los Rios, Gramine derivatives targeting Ca(2+) channels and ser/thr phosphatases: a new dual strategy for the treatment of neurodegenerative diseases, J. Med. Chem. 59 (2016) 6265–6280, https://doi.org/10.1021/acs.jmedchem.6b00478.
[55] R. Lajarin-Cuesta, R.L. Arribas, C. Nanclares, E.M. Garcia-Frutos, L. Gandia, C. de Los Rios, Design and synthesis of multipotent 3-aminomethylindoles and 7-azaindoles with enhanced protein phosphatase 2A-activating profile and neuroprotection, Eur. J. Med. Chem. 157 (2018) 294–309, https://doi.org/10.1016/j.ejmech.2018.07.030.
[56] M. Medina, J. Avila, N. Villanueva, Use of okadaic acid to identify relevant phosphoepitopes in pathology: a focus on neurodegeneration, Mar. Drugs 11 (2013) 1656–1668, https://doi.org/10.3390/md11051656.
[57] Y. Xing, Y. Xu, Y. Chen, P.D. Jeffrey, Y. Chao, Z. Lin, Z. Li, S. Strack, J.B. Stock, Y. Shi, Structure of protein phosphatase 2A core enzyme bound to tumor-inducing toxins, Cell 127 (2006) 341–353, https://doi.org/10.1016/j.cell.2006.09.025.
[58] A. Takai, M. Murata, K. Torigoe, M. Isobe, G. Mieskes, T. Yasumoto, Inhibitory effect of okadaic acid derivatives on protein phosphatases. A study on structure-affinity relationship, Biochem. J. 284 (Pt 2) (1992) 539–544, https://doi.org/10.1042/bj2840539.
[59] J. Huhn, P.D. Jeffrey, K. Larsen, T. Rundberget, F. Rise, N.R. Cox, V. Arcus, Y. Shi, C.O. Miles, A structural basis for the reduced toxicity of dinophysistoxin-2, Chem. Res. Toxicol. 22 (2009) 1782–1786, https://doi.org/10.1021/tx9001622.
[60] R.L. Arribas, A. Bordas, J. Domenech Omella, J.L. Cedillo, V. Janssens, C. Montiel, C. de Los Rios, An okadaic acid fragment analogue prevents nicotine-induced resistance to cisplatin by recovering PP2A activity in non-small cell lung cancer cells, Bioorg. Chem. 100 (2020), 103874, https://doi.org/10.1016/j.bioorg.2020.103874.
[61] Y. Ichikawa, M. Isobe, T. Goto, Synthesis of a marine polyether toxin, okadaic acid. II. Synthesis of segment B, Tetrahedron 43 (1987) 4749–4758, https://doi.org/10.1016/S0040-4020(01)86916-7.
[62] C.J. Forsyth, S.F. Sabes, R.A. Urbanek, An efficient total synthesis of okadaic acid, J. Am. Chem. Soc. 119 (1997) 8381–8382, https://doi.org/10.1021/ja9715206.
[63] H. Fuwa, K. Sakamoto, T. Muto, M. Sasaki, Concise synthesis of the C15-C38 fragment of okadaic acid: application of the Suzuki-Miyaura reaction to spiroacetal synthesis, Org. Lett. 17 (2015) 366–369, https://doi.org/10.1021/ol503491t.
[64] Y. Pang, C. Fang, M.J. Twiner, C.O. Miles, C.J. Forsyth, Total synthesis of dinophysistoxin-2 and 2-epi-dinophysistoxin-2 and their PPase inhibition, Angew Chem. Int. Ed. Engl. 50 (2011) 7631–7635, https://doi.org/10.1002/anie.201101741.
[65] H. Becker, K.B. Sharpless, A new ligand class for the asymmetric dihydroxylation of olefins, Angew Chem. Int. Ed. Engl. 35 (1996) 448–451, https://doi.org/10.1002/anie.199604481.
[66] E.R. Zimmer, E. Kalinine, C.B. Haas, V.R. Torrez, D.O. Souza, A.P. Muller, L. V. Portela, Pretreatment with memantine prevents Alzheimer-like alterations induced by intrahippocampal okadaic acid administration in rats, Curr. Alzheimer Res. 9 (2012) 1182–1190, https://doi.org/10.2174/156720512804142877.
[67] P.K. Kamat, S. Rai, C. Nath, Okadaic acid induced neurotoxicity: an emerging tool to study Alzheimer's disease pathology, Neurotoxicology 37 (2013) 163–172, https://doi.org/10.1016/j.neuro.2013.05.002.
[68] M.R. Swingle, L. Amable, B.G. Lawhorn, S.B. Buck, C.P. Burke, P. Ratti, K. L. Fischer, D.L. Boger, R.E. Honkanen, Structure-activity relationship studies of fostriecin, cytostatin, and key analogs, with PP1, PP2A, PP5, and(beta12-beta13)-chimeras (PP1/PP2A and PP5/PP2A), provide further insight into the inhibitory actions of fostriecin family inhibitors, J. Pharmacol. Exp. Therapeut. 331 (2009) 45–53, https://doi.org/10.1124/jpet.109.155630.
[69] E. Ramos, R. Lajarin-Cuesta, R.L. Arribas, E.M. Garcia-Frutos, L. Gonzalez-Lafuente, J. Egea, C. de Los Rios, A. Romero, In silico prediction of the toxic potential of neuroprotective bifunctional molecules based on chiral N-Propargyl-

1,2-amino alcohol derivatives, Chem. Res. Toxicol. 34 (2021) 1245–1249, https://doi.org/10.1021/acs.chemrestox.0c00519.
[70] A. Romero, J. Egea, A.G. Garcia, M.G. Lopez, Synergistic neuroprotective effect of combined low concentrations of galantamine and melatonin against oxidative stress in SH-SY5Y neuroblastoma cells, J. Pineal Res. 49 (2010) 141–148, https://doi.org/10.1111/j.1600-079X.2010.00778.x.
[71] J. Lewerenz, P. Maher, Chronic glutamate toxicity in neurodegenerative diseases-what is the evidence? Front. Neurosci. 9 (2015) 469, https://doi.org/10.3389/fnins.2015.00469.
[72] E.R. Zimmer, A. Leuzy, D.O. Souza, L.V. Portela, Inhibition of protein phosphatase 2A: focus on the glutamatergic system, Mol. Neurobiol. (2015) 3753–3755, https://doi.org/10.1007/s12035-015-9321-0.
[73] Z.W. Sun, L. Zhang, S.J. Zhu, W.C. Chen, B. Mei, Excitotoxicity effects of glutamate on human neuroblastoma SH-SY5Y cells via oxidative damage, Neurosci. Bull. 26 (2010) 8–16, https://doi.org/10.1007/s12264-010-0813-7.
[74] U.Y. Yu, B.C. Yoo, J.H. Ahn, Regulatory B subunits of protein phosphatase 2A are involved in site-specific regulation of tau protein phosphorylation, KOREAN J. PHYSIOL. PHARMACOL. 18 (2014) 155–161, https://doi.org/10.4196/kjpp.2014.18.2.155.
[75] C. Letourneux, G. Rocher, F. Porteu, B56-containing PP2A dephosphorylate ERK and their activity is controlled by the early gene IEX-1 and ERK, EMBO J. 25 (2006) 727–738, https://doi.org/10.1038/sj.emboj.7600980.
[76] J.Z. Wang, I. Grundke-Iqbal, K. Iqbal, Kinases and phosphatases and tau sites involved in Alzheimer neurofibrillary degeneration, Eur. J. Neurosci. 25 (2007) 59–68, https://doi.org/10.1111/j.1460-9568.2006.05226.x.
[77] L. Di, E.H. Kerns, K. Fan, O.J. McConnell, G.T. Carter, High throughput artificial membrane permeability assay for blood-brain barrier, Eur. J. Med. Chem. 38 (2003) 223–232, https://doi.org/10.1016/s0223-5234(03)00012-6.
[78] G. Patlewicz, N. Jeliazkova, R.J. Safford, A.P. Worth, B. Aleksiev, An evaluation of the implementation of the Cramer classification scheme in the Toxtree software, SAR QSAR Environ. Res. 19 (2008) 495–524, https://doi.org/10.1080/10629360802083871.
[79] R. Singh, S. Thota, R. Bansal, Studies on 16,17-pyrazoline substituted heterosteroids as anti-alzheimer and anti-parkinsonian agents using LPS induced neuroinflammation models of mice and rats, ACS Chem. Neurosci. 9 (2018) 272–283, https://doi.org/10.1021/acschemneuro.7b00303.
[80] G.C. Brown, The endotoxin hypothesis of neurodegeneration, J. Neuroinflammation 16 (2019) 180, https://doi.org/10.1186/s12974-019-1564-7.
[81] L.E. Gardner, J.D. White, M.J. Eimerbrink, G.W. Boehm, M.J. Chumley, Imatinib methanesulfonate reduces hyperphosphorylation of tau following repeated peripheral exposure to lipopolysaccharide, Neuroscience 331 (2016) 72–77, https://doi.org/10.1016/j.neuroscience.2016.06.007.
[82] J.N. Manda, B.B. Butler Jr., A. Aponick, Synthesis and biological evaluation of the southern hemisphere of Spirastrellolide A and analogues, J. Org. Chem. 85 (2020) 13694–13709, https://doi.org/10.1021/acs.joc.0c01867.
[83] C.D. Liu, Q. Wang, D.K. Zong, S.C. Pei, Y. Yan, M.L. Yan, L.L. Sun, Y.Y. Hao, M. Mao, W.J. Xing, H. Ren, J. Ai, Knockdown of microRNA-195 contributes to protein phosphatase-2A inactivation in rats with chronic brain hypoperfusion, Neurobiol. Aging 45 (2016) 76–87, https://doi.org/10.1016/j.neurobiolaging.2016.05.010.
[84] H.J. Park, K.W. Lee, E.S. Park, S. Oh, R. Yan, J. Zhang, T.G. Beach, C.H. Adler, M. Voronkov, S.P. Braithwaite, J.B. Stock, M.M. Mouradian, Dysregulation of protein phosphatase 2A in Parkinson disease and dementia with lewy bodies, Ann Clin. Transl. Neurol. 3 (2016) 769–780, https://doi.org/10.1002/acn3.337.
[85] W.J. Yang, W. Chen, L. Chen, Y.J. Guo, J.S. Zeng, G.Y. Li, W.S. Tong, Involvement of tau phosphorylation in traumatic brain injury patients, Acta Neurol. Scand. 135 (2017) 622–627, https://doi.org/10.1111/ane.12644.
[86] B. Adhikari, B. De Silva, J.A. Molina, A. Allen, S.H. Peck, S.Y. Lee, Neuronal ceroid lipofuscinosis related ER membrane protein CLN8 regulates PP2A activity and ceramide levels, Biochim. Biophys. Acta, Mol. Basis Dis. 1865 (2019) 322–328, https://doi.org/10.1016/j.bbadis.2018.11.011.
[87] T. Lu, R. Chen, T.C. Cox, R.X. Moldrich, N. Kurniawan, G. Tan, J.K. Perry, A. Ashworth, P.F. Bartlett, L. Xu, J. Zhang, B. Lu, M. Wu, Q. Shen, Y. Liu, L. J. Richards, Z. Xiong, X-linked microtubule-associated protein, Mid1, regulates axon development, Proc. Natl. Acad. Sci. U. S. A. 110 (2013) 19131–19136, https://doi.org/10.1073/pnas.1303687110.
[88] M. Arif, S.F. Kazim, I. Grundke-Iqbal, R.M. Garruto, K. Iqbal, Tau pathology involves protein phosphatase 2A in parkinsonism-dementia of Guam, Proc. Natl. Acad. Sci. USA 111 (2014) 1144–1149, https://doi.org/10.1073/pnas.1322614111.
[89] X.L. Tan, D.K. Wright, S. Liu, C. Hovens, T.J. O'Brien, S.R. Shultz, Sodium selenate, a protein phosphatase 2A activator, mitigates hyperphosphorylated tau and improves repeated mild traumatic brain injury outcomes, Neuropharmacology 108 (2016) 382–393, https://doi.org/10.1016/j.neuropharm.2016.05.001.
[90] R. Yan, J. Zhang, H.J. Park, E.S. Park, S. Oh, H. Zheng, E. Junn, M. Voronkov, J. B. Stock, M.M. Mouradian, Synergistic neuroprotection by coffee components eicosanoyl-5-hydroxytryptamide and caffeine in models of Parkinson's disease and DLB, Proc. Natl. Acad. Sci. U. S. A. 115 (2018) E12053–E12062, https://doi.org/10.1073/pnas.1813365115.
[91] F.A. Shah, D.J. Park, S.A. Gim, P.O. Koh, Curcumin treatment recovery the decrease of protein phosphatase 2A subunit B induced by focal cerebral ischemia in Sprague-Dawley rats, Lab Anim. Res. 31 (2015) 134–138, https://doi.org/10.5625/lar.2015.31.3.134.
[92] M.E. Prados, A. Correa-Saez, J.D. Unciti-Broceta, M. Garrido-Rodriguez, C. Jimenez-Jimenez, M. Mazzone, A. Minassi, G. Appendino, M.A. Calzado, E. Munoz, Betulinic acid hydroxamate is neuroprotective and induces protein phosphatase 2A-dependent HIF-1alpha stabilization and post-transcriptional dephosphorylation of prolyl hydrolase 2, Neurotherapeutics 18 (2021) 1849–1861, https://doi.org/10.1007/s13311-021-01089-4.
[93] R. Nakamura, K. Tanino, M. Miyashita, Total synthesis of scytophycin C. 1. Stereoselective syntheses of the C(1)-C(18) segment and the C(19)-C(31) segment, Org. Lett. 5 (2003) 3579–3582, https://doi.org/10.1021/ol035227o.
[94] K.C. Nicolaou, M.E. Duggan, C.K. Hwang, Synthesis of the ABC ring system of brevetoxin B, J. Am. Chem. Soc. 111 (1989) 6666–6675, https://doi.org/10.1021/ja00199a029.
[95] L. Viejo, M. Rubio-Alarcon, R.L. Arribas, M. Moreno-Castro, R. Perez-Marin, M. Braun-Cornejo, M. Estrada-Valencia, C. de Los Rios, Synthesis and biological assessment of 4,1-benzothiazepines with neuroprotective activity on the Ca(2+) overload for the treatment of neurodegenerative diseases and stroke, Molecules 26 (2021) 4473, https://doi.org/10.3390/molecules26154473.
[96] R. Thomsen, M.H. Christensen, MolDock, A new technique for high-accuracy molecular docking, J. Med. Chem. 49 (2006) 3315–3321, https://doi.org/10.1021/jm051197e.
[97] F. Calzaferri, P. Narros-Fernandez, R. de Pascual, A.M.G. de Diego, A. Nicke, J. Egea, A.G. Garcia, C. de Los Rios, Synthesis and pharmacological evaluation of novel non-nucleotide purine derivatives as P2X7 antagonists for the treatment of neuroinflammation, J. Med. Chem. 64 (2021) 2272–2290, https://doi.org/10.1021/acs.jmedchem.0c02145.